Combining near-infrared fluorescence with Brainbow to visualize expression of specific genes within a multicolor context

Zoe T. Cook, Nicole L. Brockway, Zachary J. C. Tobias, Joy Pajarla, Isaac S. Boardman, Helen Ippolito, Sylvia Nkombo Nkoula, and Tamily A. Weissman*
Biology Department, Lewis and Clark College, Portland, OR 97219

ABSTRACT **Fluorescent proteins are a powerful experimental tool, allowing the visualization of gene expression and cellular behaviors in a variety of systems. Multicolor combinations of fluorescent proteins, such as Brainbow, have expanded the range of possible research questions and are useful for distinguishing and tracking cells. The addition of a separately driven color, however, would allow researchers to report expression of a manipulated gene within the multicolor context to investigate mechanistic effects. A far-red or near-infrared protein could be particularly suitable in this context, as these can be distinguished spectrally from Brainbow. We investigated five far-red/near-infrared proteins in zebrafish: TagRFP657, mCardinal, miRFP670, iRFP670, and mIFP. Our results show that both mCardinal and iRFP670 are useful fluorescent proteins for zebrafish expression. We also introduce a new transgenic zebrafish line that expresses Brainbow under the control of the neuroD promoter. We demonstrate that mCardinal can be used to track the expression of a manipulated bone morphogenetic protein receptor within the Brainbow context. The overlay of near-infrared fluorescence onto a Brainbow background defines a clear strategy for future research questions that aim to manipulate or track the effects of specific genes within a population of cells that are delineated using multicolor approaches.**

Monitoring Editor
Diane Lidke
University of New Mexico

Received: Jun 4, 2018
Revised: Dec 13, 2018
Accepted: Dec 18, 2018

INTRODUCTION

Fluorescent proteins (FPs) have revolutionized cellular and molecular biology, allowing the in vivo visualization of cells, organelles, and proteins via fluorescence microscopy. Derived via mutagenesis to protein templates found primarily in marine invertebrate species (see Shimomura *et al.*, 1962; Heim *et al.*, 1994; Matz *et al.*, 1999), FPs function as a precise and minimally invasive labeling method commonly used in a variety of experimental systems (reviewed in Shimomura, 2005; Giepmans *et al.*, 2006; Kremers *et al.*, 2011; Toseland, 2013). The diversity in excitation and emission spectra among FPs allows for novel, multicolor techniques (reviewed in Shaner *et al.* 2005; Day and Davidson, 2009; Rodriguez *et al.*, 2017). For example, the Brainbow cell-labeling techniques use three (or in some cases four) different fluorescent proteins to label cells of the same population with hues across the visible spectrum (Livet *et al.*, 2007; Cai *et al.*, 2013; Pan *et al.*, 2013). Multiple copies of the Brainbow transgene are expressed within each cell, and the color expressed by each copy is randomly determined by the action of Cre recombinase; this results in unique, combinatorial colors that distinguish among *like* cells (Livet *et al.*, 2007; reviewed in Weissman and Pan, 2015). Several other multicolor approaches have been developed as well (e.g., Boldogkoi *et al.*, 2009; Snippert *et al.*, 2010; Distel *et al.*, 2011; Weber *et al.*, 2011; Malide *et al.*, 2012; Worley *et al.*, 2013; Garcia-Marques *et al.*, 2014; Garcia-Moreno *et al.*, 2014; Nern *et al.*, 2015; Pontes-Quero *et al.*, 2017); all of which are suitable for studying cellular interactions and dynamics in various systems. Multicolor labeling is particularly informative in studies of clonal relationships during development; for example, in Brainbow, daughter cells retain the unique fluorescent coloring of their parent cell (Gupta and Poss, 2012; Pan *et al.*, 2013; Loulier *et al.*, 2014),

This article was published online ahead of print in MBoC in Press (http://www.molbiolcell.org/cgi/doi/10.1091/mbc.E18-06-0340) on December 26, 2018.
*Address correspondence to: Tamily A. Weissman (weissman@lclark.edu).
Abbreviation used: FP, fluorescent protein.

allowing cell lineage to be traced and clones to be identified within a living, growing organism (Weissman and Pan, 2015).

While multicolor approaches such as Brainbow are useful, their combination with the expression of a separately driven, spectrally distinct FP has the potential to significantly broaden the range of possible experiments. For example, a distinct FP tagged to a specific protein would allow assessment of that protein's function, either within a population (or subset) of Brainbow-labeled cells, or in a separate population of cells. Since the spectra of the FPs used in Brainbow already span the majority of the visible range of light (e.g., Brainbow versions 1.0–3.2; Livet *et al.,* 2007; Cai *et al.,* 2013), it is advantageous to consider complementary FPs whose spectra lie in the far-red and/or near-infrared region (where 650 nm is an approximate boundary between far-red <650, and near-infrared >650; Filonov *et al.,* 2011; reviewed in Chernov *et al.,* 2017). This strategy has been utilized in calcium imaging, where a far-red calcium indicator was generated for use in multicolor contexts (Egawa *et al.,* 2011). Importantly, the longer wavelengths in far-red and near-infrared fluorescence are of lower energy and can penetrate deeper in comparison to visible light (Ntziachristos *et al.,* 2003; Deliolanis *et al.,* 2008).

Here we establish a strategy for combining Brainbow with the simultaneous expression of a visually distinct far-red or near-infrared fluorescent protein. This combinatorial approach allows the visualization of a population of cells coupled with the additional tagging of a specific protein or cell type, ultimately expanding the types of questions that can be answered using multicolor labeling. In demonstrating the feasibility of this experimental strategy, we also identify one useful far-red fluorescent protein and one useful near-infrared fluorescent protein for use in zebrafish (*Danio rerio*), a powerful system for fluorescence imaging (Ko *et al.,* 2011; Weber and Köster, 2013), in which Brainbow has been used to study the nervous system, circulatory system, immune system, and beyond (Kinkhabwala *et al.,* 2011; Pan *et al.,* 2011, 2013; Gupta and Poss, 2012; Heap *et al.,* 2013; Kochhan *et al.,* 2013; Robles *et al.,* 2013; Dirian *et al.,* 2014; Pagán *et al.,* 2015; Xiong *et al.,* 2015; Avagyan *et al.,* 2016; Chen *et al.,* 2016a,b; Foglia *et al.,* 2016; Han *et al.,* 2016; Albadri *et al.,* 2017; Furlan *et al.,* 2017; Henninger *et al.,* 2017; Herget *et al.,* 2017; Singh *et al.,* 2017; Kesavan *et al.,* 2018).

Owing to the diversity in available far-red and near-infrared FPs, and the variation in FP performance among different experimental systems, we first perform a quantitative comparison of the expression of five different far-red and near-infrared FPs in vivo. There are numerous factors that affect the suitability of a given fluorescent protein for a particular system, including imaging conditions, photochemical properties of the protein, and intrinsic cellular properties of the model organism (Heppert *et al.,* 2016). While the inherent brightness of an FP can be predicted, the actual brightness may vary in vivo based on expression level, transcript/protein stability, fluorophore maturation rate, and autofluorescence within the specific host organism (Heppert *et al.,* 2016). Additionally, for experiments requiring time-lapse imaging, the rate of photobleaching, which can vary significantly among FPs, is an important consideration (Shaner *et al.,* 2005). Finally, though rare, some FPs may induce unwanted cytotoxic effects, particularly if they are oligomeric (Shaner *et al.,* 2005; Ansari *et al.,* 2016). For these reasons, we quantified the in vivo performance of several FPs in zebrafish to determine which is the brightest, most photostable, and least toxic for use in future studies. We also introduce a new transgenic line of zebrafish expressing Brainbow in the developing nervous system and demonstrate that the brightest of the FPs assessed, mCardinal, can be used to tag and visualize a manipulated protein within this multicolor background.

RESULTS

Selection and expression of far-red and near-infrared FP candidates in zebrafish

To assess which fluorescent proteins could be used as a complement to Brainbow studies in zebrafish, we initially selected proteins that are excited by the 633-nm laser line of our confocal microscope, a common laser line for far-red and near-infrared fluorophore excitation (Morozova *et al.,* 2010). Additionally, we selected proteins that are not photoactivatable or photoconvertable, as the light exposure from Brainbow imaging could unintentionally alter those types of FPs. We preferentially selected monomeric proteins, as they have a reduced potential for toxicity and can be used in fusion proteins without causing unintended oligomerization (Shaner *et al.,* 2005). On this basis, we compared five FPs: mCardinal (Chu *et al.,* 2014), TagRFP657 (Morozova *et al.,* 2010), miRFP670 (Shcherbakova *et al.,* 2016), iRFP670 (Shcherbakova and Verkhusha, 2013), and mIFP (Yu *et al.,* 2015) (Table 1). Both mCardinal and TagRFP657 are excited in the far-red range (peaks at 604 and 611 nm, respectively) but emit in the near-infrared range above 650 nm (659 and 657, respectively). In contrast, miRFP670, iRFP670, and mIFP are considered true near-infrared FPs, because both their emission and excitation spectra fall close to or above 650 nm.

Of the five selected proteins, mCardinal and TagRFP657 were both derived from several rounds of mutagenesis to the GFP-like protein eqFP578 from the sea anemone *Entacmaea quadricolor* (Shcherbo *et al.,* 2007; Morozova *et al.,* 2010; Chu *et al.,* 2014), while miRFP670, iRFP670, and mIFP were created using bacterial phytochromes as templates (Shcherbakova and Verkhusha, 2013; Shcherbakova *et al.,* 2016; Yu *et al.,* 2015). TagRFP657 was engineered directly from mutagenesis to an earlier FP, mKate (Morozova *et al.,* 2010). mKate was also used as a template for Neptune (Lin *et al.,* 2009), the immediate FP predecessor of mCardinal (Chu *et al.,* 2014). mIFP was created via mutagenesis to *Br*BphP (Yu *et al.,* 2015), a bacterial phytochrome found in *Bradyrhizobium*, where it regulates the synthesis of the photosynthetic apparatus in response to light (Giraud *et al.,* 2002). iRFP670 was also derived from a bacterial phytochrome template, specifically *Rp*BphP6 (Shcherbakova and Verkhusha, 2013) from the bacteria *Rhodopseudomonas palustris* (Giraud and Verméglio, 2008). Compared to the other proteins, which are monomeric and thus more likely to be nontoxic and not interfere with fusion protein function, iRFP670 is known to dimerize (Shcherbakova and Verkhusha, 2013). In contrast, miRFP670 is a monomeric FP engineered from *Rp*BphP1 (Shcherbakova *et al.,* 2016), another bacterial phytochrome found in *R. palustris* (Bellini and Papiz, 2012), with similar spectral properties.

To assess the suitability of each FP for developmental Brainbow studies, we constructed plasmids for their expression in zebrafish utilizing the hsp70 promoter and SV40 late polyadenylation signal. The hsp70 promoter is an ~1.5-kb fragment that drives the expression of an endogenous heat-inducible zebrafish gene (Halloran *et al.,* 2000); it can thus be utilized to induce the robust expression of a downstream transgene in zebrafish embryos exposed to 37°C. This promoter is useful in inducing transient ectopic expression throughout zebrafish embryos following microinjection, providing an efficient means of assessing gene function without cell-type-specific promoters. Additionally, it allows a high level of temporal control over gene expression, avoiding potentially confounding effects of a transgene on early development (Shoji and Sato-Maeda, 2008).

We utilized microinjections to transiently express each far-red/near-infrared FP plasmid in zebrafish embryos and then visualized the heat-induced expression via in vivo confocal microscopy at 2 d postfertilization (dpf). As expected, the hsp70 promoter drove

Protein	Excitation maximum (nm)	Emission maximum (nm)	Oligomerization state	Fluorophore	Previous zebrafish expression	Predicted brightness using 633 nm laser (M^{-1} cm^{-1})	Predicted brightness using 647 nm laser (M^{-1} cm^{-1})	Codon Adaptation index (CAI) for zebrafish expression
mCardinal	604	659	Monomer	Autocatalytic	Yes (Gupta *et al.*, 2018)	2888	789	0.878
TagRFP657	611	657	Monomer	Autocatalytic	No	1457	433	0.873
miRFP670	642	670	Monomer	Biliverdin	No	10,324	10,337	0.750
iRFP670	643	670	Dimer	Biliverdin	Yes (Ando *et al.*, 2016)	10,728	11,035	0.759
mIFP	683	704	Monomer	Biliverdin	Yes (Yu *et al.*, 2015)	3005	3655	0.795

TABLE 1: Far-red and near-infrared fluorescent proteins evaluated and relevant properties.

ectopic expression of mCardinal, TagRFP657, miRFP670, iRFP670, and mIFP throughout fish (Figure 1), consistently labeling a variety of cell types, including neurons (Figure 2) and muscle (Figure 3). To ensure that the near-infrared fluorescence observed was due to the FP and not autofluorescence, we also imaged wild-type zebrafish in an identical manner (Supplemental Figure 1). Autofluorescence was consistently observed in cells within the yolk, distal tail, and developing retinal pigmented epithelium in wild-type fish but not in the cell types typically targeted by hsp70. Moreover, assessment for cytotoxic effects of FP expression showed that expression did not result in punctate labeling, which can indicate cell death or lysosomal aggregation of the FP (Katayama *et al.* 2008; Shemiakina *et al.*, 2012).

Quantification of far-red and near-infrared fluorescent protein brightness

Before measuring brightness in vivo, we determined a predicted brightness for each FP calculated for our imaging settings (Heppert *et al.*, 2016), using the quantum yield, extinction coefficient, and excitation/emission spectra as reported (Morozova *et al.*, 2010; Shcherbakova and Verkhusha, 2013; Shcherbakova *et al.*, 2016; Chu *et al.*, 2014; Yu *et al.*, 2015) (Figure 4). This value takes into account intrinsic properties of the fluorophore as well as the specific laser line used for excitation and the range of wavelengths collected to predict what maximal brightness would be expected under given imaging conditions. Of the FPs considered, miRFP670 and iRFP670 were predicted to be brightest (10,324 and 10,728 M^{-1} cm^{-1}, respectively) by a factor of ~3.5 in comparison to the next brightest, mIFP (3005 M^{-1} cm^{-1}). mIFP was predicted to be only slightly brighter than mCardinal (2977 M^{-1} cm^{-1}), while TagRFP657 (1457 M^{-1} cm^{-1}) was predicted to be less than half as bright as mIFP and mCardinal (Figure 4C). For our experiments we utilized a 633 nm laser line; Table 1 also provides the predicted brightness values for excitation at 647 nm.

Brightness is a key factor in determining which FP is ideal for in vivo expression. To compare in vivo brightness among the five FPs expressed, measurements of mean brightness were taken from images of cells in the hindbrain and muscle cells of the tail (Figure 5) in living zebrafish. While the brightness of both hindbrain and muscle cells varied within and among conditions, mean normalized fluorescence intensity of fish expressing mCardinal was highest in both hindbrain cells (Figure 5C; mCardinal: 125.6 ± 14.6 AU, n = 935 cells from 24 fish; TagRFP657: 26.2 ± 3.0, n = 580 cells from 25 fish; miRFP670: 16.6 ± 2.7, n = 60 cells from seven fish; iRFP670: 24.5 ± 3.1, n = 325 cells from 12 fish; mIFP: 11.2 ± 1.2, n = 137 cells from 20 fish) and muscle cells (Figure 5D; mCardinal: 193.5 ± 34.5 AU, n = 272 cells from 18 fish; TagRFP657: 43.9 ± 8.3, n = 188 cells from 23 fish; miRFP670: 8.7 ± 1.3, n = 28 cells from five fish; iRFP670: 24.9 ± 3.7, n = 15 cells from four fish; mIFP: 7.4 ± 0.94, n = 91 cells from 17 fish). Addition of heme oxygenase did not significantly alter brightness measurements for miRFP670. iRFP670, or mIFP (unpublished data). mCardinal was significantly brighter than all other FPs tested in both hindbrain neurons ($F_{4, 83} = 32.56$, $p < 1.0 \times 10^{-7}$; all Tukey HSD $p < 1.0 \times 10^{-7}$) and muscle cells ($F_{4, 74} = 18.59$, $p < 1.0 \times 10^{-7}$; all Tukey HSD $p < 5.0 \times 10^{-5}$), and no other FPs differed in brightness from one another (all Tukey HSD $p > 0.5$).

Photobleaching analysis

One characteristic of FPs that affects their performance in vivo is how readily they photobleach. FPs that bleach quickly are less useful for in vivo studies, regardless of their brightness. To assess the suitability of each FP for time-lapse imaging experiments, its rate of

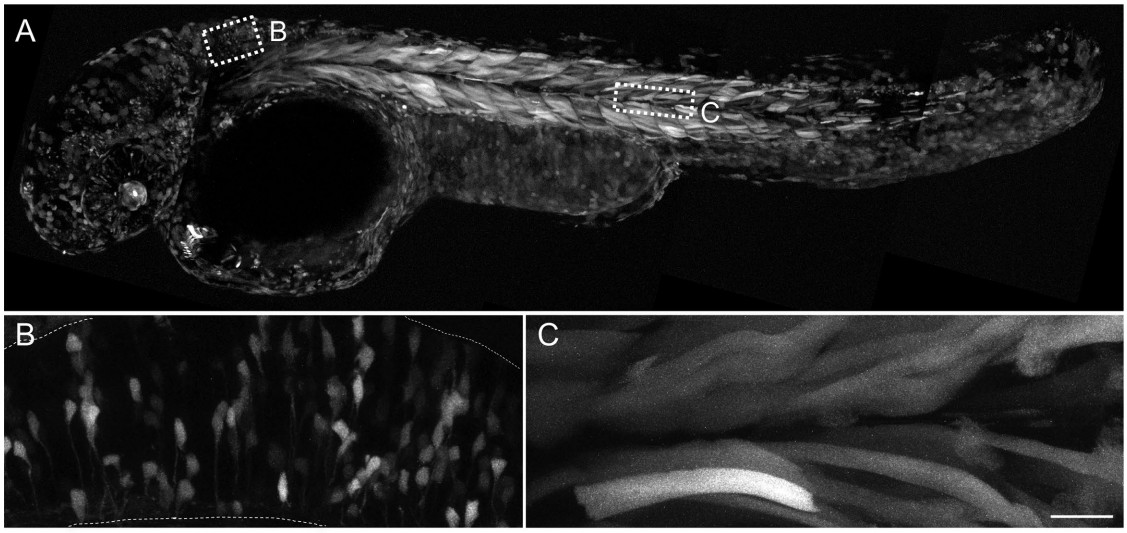

FIGURE 1: Far-red and near-infrared FPs can be expressed and visualized in zebrafish embryos. (A) In vivo mCardinal expression in whole embryo at 2 dpf. Montage of five maximum intensity projections stitched together; display levels for A only have been adjusted both linearly and nonlinearly to optimize stitching and viewing. Boxes indicate general hindbrain and muscle regions where images such as B and C were taken. (B) Maximum intensity projection showing 2 dpf zebrafish hindbrain expressing mCardinal. Projection contains 24 slices for a total depth of 21.5 µm. Dotted lines show approximate extent of hindbrain. (C) Maximum intensity projection showing muscle cells of zebrafish shown in A. Projection contains 41 slices for a total depth of 36.8 µm. In B and C, brightness was adjusted linearly and identically for display. In all panels, dorsal is up and rostral is to the left. Scale bar represents 25 µm in B and C.

photobleaching was assessed by continuous imaging of a single hindbrain cell at high laser power (Figure 6). For these experiments we used a laser power significantly higher (70%) than what is needed for typical imaging conditions (<10%); this allowed us to test the performance of each FP under extreme conditions.

TagRFP657 demonstrated the lowest relative level of photobleaching, maintaining a mean of 91% (±1.2; $n = 5$ cells) of its original fluorescence after 2 min of bleaching at high laser power, while miRFP670 bleached slightly more rapidly, retaining 83% of its initial fluorescence over time (±2.2; $n = 6$ cells). mCardinal and mIFP bleached at similar rates, depreciating to 71% (±1.4; $n = 5$ cells) and 72% (±1.7; $n = 4$ cells) of their original brightness respectively. iRFP670 displayed the highest level of photobleaching of the FPs assessed; over the course of imaging, its fluorescence decayed to

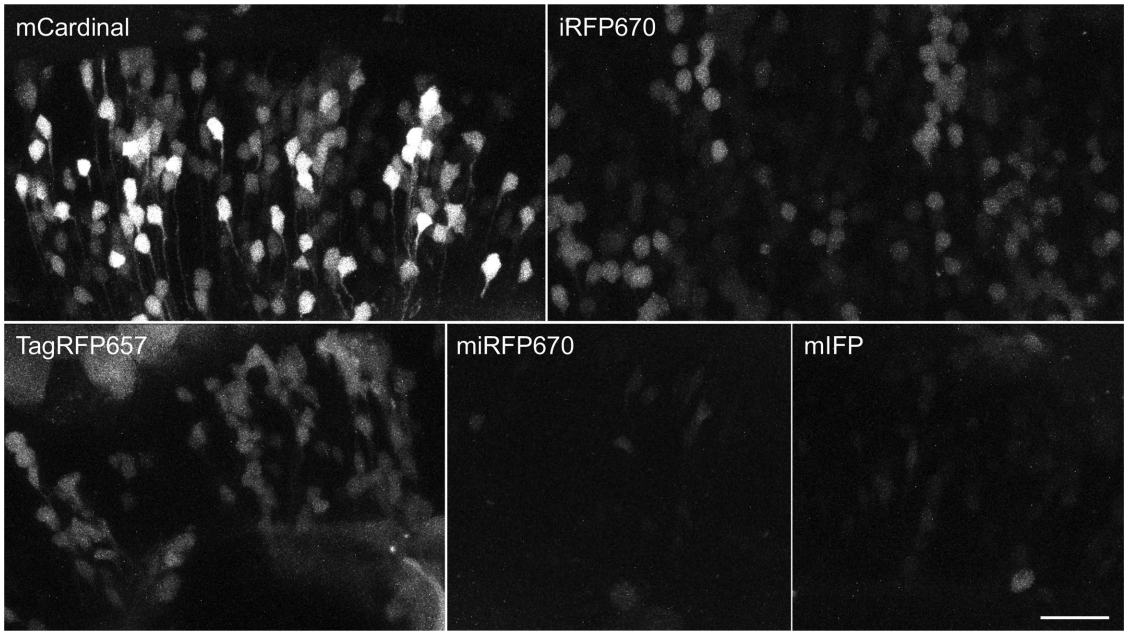

FIGURE 2: Far-red and near-infrared FPs express in the developing zebrafish hindbrain. In vivo hindbrain expression is shown in 2 dpf embryos expressing either mCardinal, iRFP670, TagRFP657, miRFP670, or mIFP. In all panels, dorsal is up and rostral is to the left, and image is a maximum intensity projection representing 33–35 slices for a total depth of ~30 µm. The same acquisition parameters were used for each image and brightness was linearly adjusted for display (identical adjustments for each frame). Scale bar represents 25 µm.

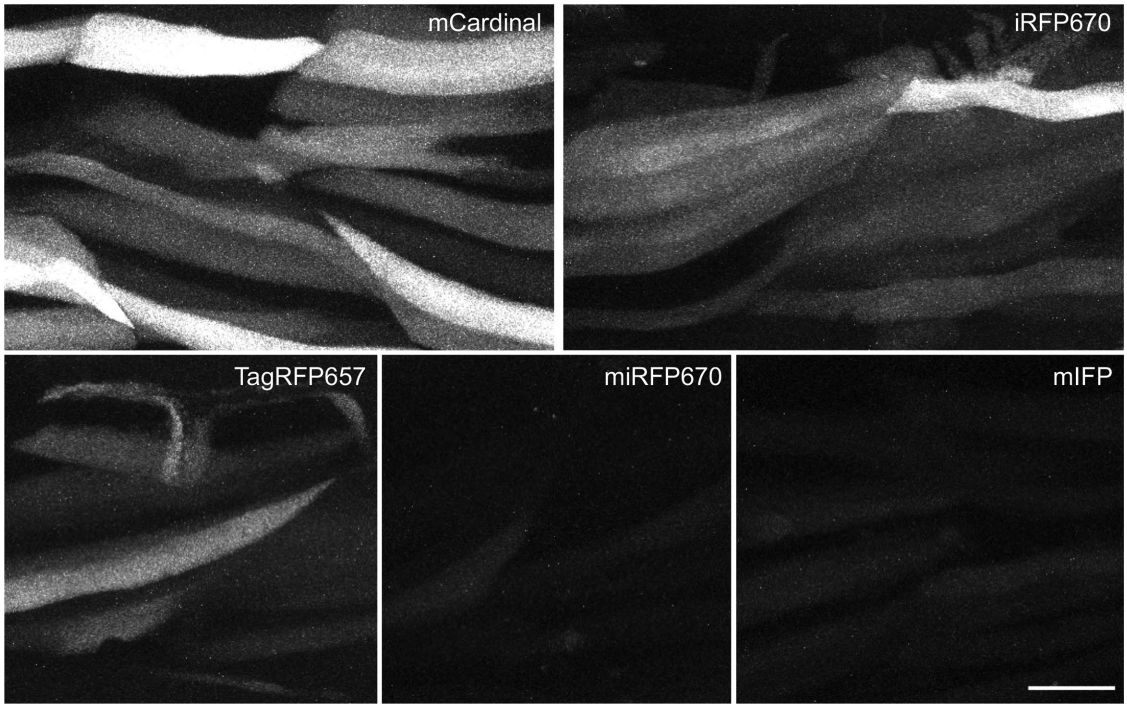

FIGURE 3: Far-red and near-infrared FPs express in muscle cells within the tail of developing zebrafish. In vivo expression in muscle cells is shown in 2 dpf embryos expressing either mCardinal, iRFP670, TagRFP657, miRFP670, or mIFP. In all panels, dorsal is up and rostral is to the left, and image is a maximum intensity projection representing 25–35 slices for a total depth of ~20–30 µm. The same acquisition parameters were used for each image and brightness was linearly adjusted for display (identical adjustments for each frame). Scale bar represents 25 µm.

42% of initial brightness (±2.8; n = 5 cells) (Figure 6B). Because mCardinal demonstrated a much higher initial brightness than TagRFP657, miRFP670, iRFP670, or mIFP (see Figure 5), when each FP was normalized to the initial brightness of mCardinal, all other FPs tested were dimmer throughout the entire course of imaging.

Coexpression of an mCardinal-tagged protein with Brainbow

To demonstrate the feasibility of a combinatorial Brainbow and far-red/near-infrared FP expression strategy, we next tested whether a fourth FP could be distinguished from Brainbow expression in vivo (Figure 7). After identifying mCardinal to be the overall brightest of the FPs assessed and sufficiently photostable and nontoxic for experimental purposes, we coexpressed this FP with Brainbow in zebrafish embryos and imaged all four fluorescent proteins in the hindbrain in vivo (Figure 7C). We repeated this strategy for our brightest bacterial phytochrome-derived near-infrared FP, iRFP670 (Figure 7D). For these experiments we used our newly generated transgenic zebrafish line *Tg(neurod:Zebrabow),* in which Brainbow (version 1.0 line L; Livet *et al.,* 2007) expression is restricted to the developing nervous system by the neuroD promoter (Obholzer *et al.,* 2008) (Figure 7A). This line was crossed to fish expressing the Cre recombinase, *Tg(hsp:Cre^{a134})*, to initiate Brainbow recombination in resulting embryos. In vivo confocal imaging of larvae coexpressing mCardinal with Brainbow allowed for clear detection of mCardinal within the multicolor background (Figure 7C). Brainbow and mCardinal were expressed in partially overlapping populations of cells. mCardinal was detectable in its own channel with no bleedthrough from any of the Brainbow channels (CFP, YFP, or dTomato). When viewing the dTomato channel, however, it was important to use a narrowed range of emission collection to exclude minimal mCardinal signal excited broadly by the 561-nm laser (see Supplemental Figure 2). When imaging iRFP670 expression with Brainbow, all four FPs were visible and distinct from one another (CFP, YFP, dTomato, and iRFP670; Figure 7D) with no detected bleedthrough in any channel (Supplemental Figure 2).

We next wished to test whether a specific protein tagged with a far-red FP could be identified within the context of Brainbow-labeled cells. Since our laboratory uses Brainbow to visualize dividing cells in the developing zebrafish hindbrain, we chose to manipulate a gene known to be expressed in and influence dividing cells, namely the membrane receptor for bone morphogenetic protein (BMPR). We generated an mCardinal-tagged form of the constitutively active bone morphogenetic protein receptor 1a (Nikaido *et al.,* 1999), *hsp70*:CA-BRIA-mCardinal, and injected DNA into *Tg(neurod:Zebrabow)* zebrafish embryos at the one-cell stage. Membrane expression of the BMP receptor was detected in vivo via its mCardinal tag in cells throughout the hindbrain (Figure 8). This expression was visually distinct from the cytosolic Brainbow labeling, which labeled a partially overlapping population of cells. Among the imaged cells, we identified those expressing only mCardinal, those expressing one or more of the Brainbow FPs, those coexpressing both Brainbow and mCardinal, and unlabeled cells. In colabeled cells, the mCardinal membrane expression was clearly identified as being in a separate subcellular compartment than the cytosolic Brainbow label (Figure 8, A and B), a distinction that has been shown to be useful in cellular identification (Garcia-Moreno *et al.,* 2014; Loulier *et al.,* 2014). This approach allows us to track the behavior of individual cells and simultaneously investigate how manipulation in BMP signaling influences a subset of those cells. This more broadly provides a useful strategy for multicolor labeling and

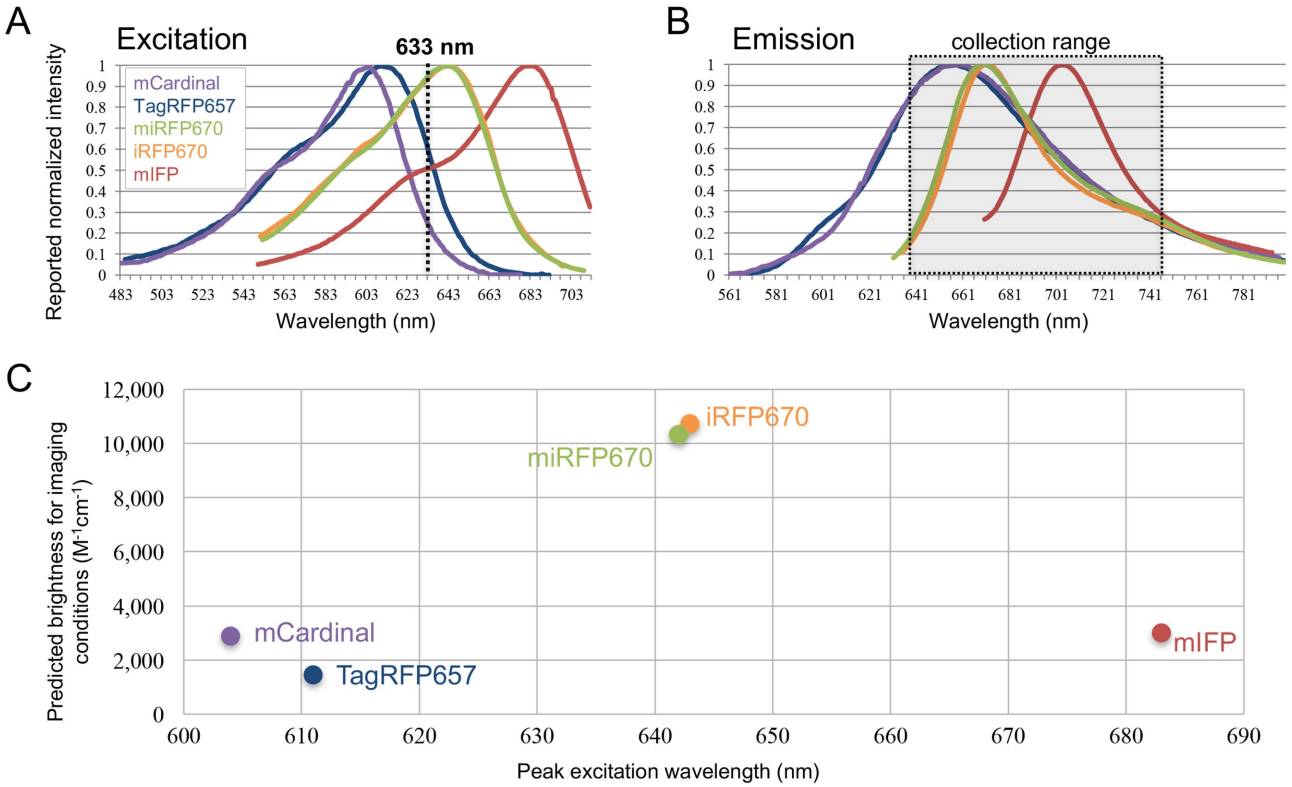

FIGURE 4: Excitation and emission spectra of far-red/near-infrared FPs can be used to predict brightness for our imaging conditions. (A) Excitation spectra and (B) emission spectra for mCardinal (purple), TagRFP657 (blue), miRFP670 (green), iRFP670 (orange), and mIFP (red) as reported, respectively, in Chu *et al.* (2014), Morozova *et al.* (2010), Shcherbakova *et al.* (2016), Shcherbakova and Verkhusha (2013), and Yu *et al.* (2016). Fluorophores were excited by a HeNe633-nm laser (vertical black line in A), and emitted light was collected between 638 and 747 nm (black box in B). (C) Predicted brightness was derived from the reported brightness (quantum yield multiplied by extinction coefficient) at the excitation wavelength of 633 nm and the portion of the emission spectra within the collection range of 638–747 nm.

clarification of dense cell populations, while simultaneously tagging, manipulating, and assessing a specific protein within that context via a fourth, visually distinct, color.

DISCUSSION

The goal of this work was to select optimal far-red or near-infrared FPs for use in conjunction with multicolor approaches such as Brainbow. Proteins that emit light in the near-infrared range can be distinguished from the FPs utilized in Brainbow 1.0–2.1 and thus provide a visually distinct label within a population of Brainbow-expressing cells. We expressed five far-red/near-infrared FPs in zebrafish and quantified the brightness and rate of photobleaching for each in vivo. After selecting mCardinal as a useful FP for zebrafish expression, we demonstrated that mCardinal can be used to tag and visualize a manipulated protein within a Brainbow background in a living zebrafish hindbrain. This establishes a clear experimental strategy for unique identification of manipulated cells within a Brainbow-labeled population.

All of the FPs we tested are relatively new and result from a recent focus on the development of red-shifted FPs that are excited by and emit longer wavelengths of light. TagRFP657, the earliest of the five FPs to have been generated (Morozova *et al.*, 2010), has been utilized in a number of studies, primarily in single-cell systems: mammalian cell cultures (e.g., Bubnell *et al.*, 2013; Cid *et al.*, 2013; Wegner *et al.*, 2017), yeast (e.g., Lee *et al.*, 2013), and *Escherichia coli* (Wu *et al.*, 2015). It has also been used in mice to label both tumors (Filonov *et al.*, 2012) and living neurons (Wegner *et al.*, 2017). In contrast, mCardinal was initially tested for in vivo performance in *Caenorhabditis elegans* and mice (Chu *et al.*, 2014) and has since been further utilized in these model organisms (*C. elegans*: Wan *et al.*, 2017; tumor-labeling in mice: Kim *et al.*, 2017; transgenic mouse line: Hirakawa *et al.*, 2018) as well as *Drosophila* (Sapar *et al.*, 2018). mCardinal has also been utilized more recently in mammalian cell culture (e.g., Alon *et al.*, 2017; Dunsing *et al.*, 2017), yeast (e.g., Syga *et al.*, 2018), and bacteria (e.g., Ghodke *et al.*, 2016), likely due to its reported higher brightness over TagRFP657 (Chu *et al.*, 2014). mCardinal has been utilized even more recently in zebrafish, in which pan-neuronal expression of mCardinal allowed researchers to construct neuroanatomical maps (Gupta *et al.*, 2018). iRFP670 was initially tested in mammalian cell culture and tumor labeling in mice (Shcherbakova and Verkhusha, 2013) and has since been utilized further in both systems (e.g., Park *et al.*, 2014; Kyung *et al.*, 2015; Rice *et al.*, 2015; Bertolin *et al.*, 2016; Zhong *et al.*, 2017; Choi *et al.*, 2018; Maass *et al.*, 2018; Mao *et al.*, 2018; Weinhard *et al.*, 2018). It has also been expressed in yeast (Bergeron *et al.*, 2017) and *E. coli* (Telford *et al.*, 2015), as well as in living mice (e.g., Martin-Lopez *et al.*, 2017; Piatkevich *et al.*, 2017), monkeys (Piatkevich *et al.*, 2017), and zebrafish (Ando *et al.*, 2016). mIFP was created more recently and was initially demonstrated to express in mice, *Drosophila*, and zebrafish (Yu *et al.*, 2015); however, it has since been applied mainly to in vitro mammalian experiments (e.g., Feng *et al.*, 2017; Shemetov *et al.*, 2017) and yeast (Dovrat *et al.*, 2018). miRFP670 is the most recently developed of these FPs; similarly to other near-infrared FPs, it was initially

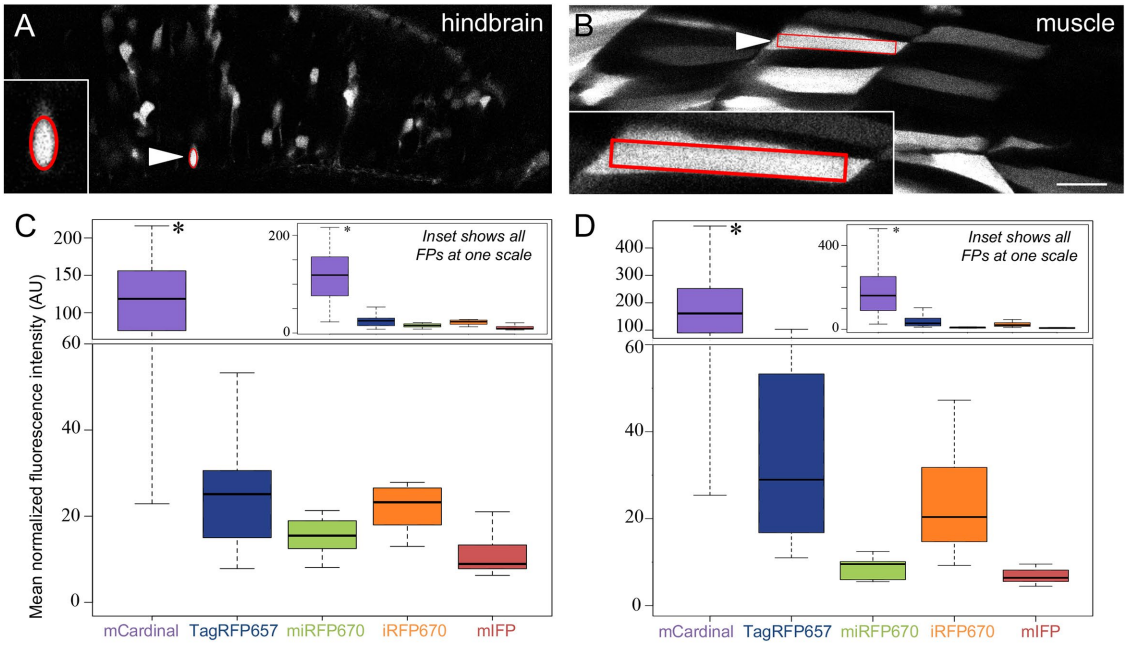

FIGURE 5: Quantified brightness of far-red and near-infrared FPs in zebrafish. (A) mCardinal expression in hindbrain, with sample region of interest shown. (B) mCardinal expression in muscle cells of the tail, with sample region of interest shown. For both A and B, dorsal is up and rostral is to the left. Elliptical regions of interest were used to select hindbrain cells, while rectangular regions of interest were used to select muscle cells. Each inset shows zoom of highlighted cell. Brightness was adjusted linearly for display. Scale bar represents 25 µm. (C, D) Average normalized fluorescence intensity per fish for each FP within the hindbrain (C) or muscle (D) cells. Scale of *y*-axis above 60 AU is condensed to optimally display both full range of mCardinal brightness and other, dimmer FPs. Insets of plots show full range of brightness at a constant scale. Whiskers show extremes of data, excluding outliers. Asterisks represent statistically significant difference brightness values from Tukey's HSD post-hoc test (all pairwise comparisons $p < 0.0000001$ for hindbrain cells and $p < 0.00005$ for muscle cells; no other significant differences).

tested in mammalian cell culture and tumors within mice (Shcherbakova *et al.*, 2016) and has since been utilized further in mammalian cell culture (e.g., Shemetov *et al.*, 2017), as well as in *E. coli* (Liu *et al.*, 2018). To our knowledge, neither TagRFP657 nor miRFP670 has been previously tested in zebrafish.

Predicted versus actual fluorescent protein brightness in zebrafish

Our results show that of the FPs we tested, mCardinal demonstrated the brightest in vivo expression in zebrafish. The brightness measurements of all FPs, however, showed significant variability in both the hindbrain (variability of mCardinal = 11.6%; TagRFP657 = 11.4%; miRFP670 = 16.1%; iRFP670 = 12.8%; and mIFP = 10.6%; standard error expressed as percent of mean brightness) and muscle cells (mCardinal = 17.8%; TagRFP657 = 19.0%; miRFP670 = 15.1%; iRFP670 = 14.8%; and mIFP = 12.7%). The range in brightness is likely due in part to the variation in zebrafish transient gene expression that results from varying amounts of injected DNA integrated into different cells (Stuart *et al.*, 1988). This could be ameliorated by generation of a stable transgenic line to assess FP expression, as genomic integration stabilizes expression across a cell population. Since we were consistent about the amount of DNA that was delivered to each egg, and each plasmid uses the same promoter that was activated by an identical heat shock protocol, the amount of underlying variability should be relatively consistent across all FP conditions. Interestingly, the range in brightness that we have quantified most likely indicates a rough range of expression that is achieved by any transient gene expression in zebrafish (Stuart *et al.*, 1990); for nonfluorescent constructs this is generally more difficult to measure.

While the brightness of all FPs varied within and between fish, the average fluorescence intensity was significantly different among FPs, with mCardinal showing the brightest in vivo expression (Figure 5). Interestingly, the greater brightness of mCardinal contrasted with its predicted brightness values, which projected miRFP670, iRFP670, and mIFP to be brighter than mCardinal. This is not unexpected; actual FP brightness has been shown to differ from predicted values in both *Saccharomyces cerevisiae* and *C. elegans* (Lee *et al.*, 2013; Heppert *et al.*, 2016), demonstrating the necessity of testing FP performance in vivo when selecting one for a particular model organism. Although the overall brightness we observed in the tested FPs did not precisely match the calculated predictions, relative brightness within each class of FP (the three bacterial phytochrome-derived near-infrared FPs vs. the two GFP-like FPs) indeed matched predicted patterns (i.e., as predicted, iRFP670 was brighter than miRFP670, which was brighter than mIFP, and mCardinal was brighter than TagRFP657). One factor that may have decreased the brightness of all of the phytochrome-derived FPs is the limited availability in zebrafish of biliverdin, the metabolite that is required to form the fluorophore (Rockwell *et al.*, 2006; Scheer and Zhao, 2008; Auldridge and Forest, 2011; Shcherbakova *et al.*, 2015). Insufficient biliverdin would diminish the brightness of miRFP670, iRFP670, and mIFP but would not affect other FPs such as TagRFP657 and mCardinal. Previous work expressing bacterial phytochrome-derived FPs in zebrafish coexpressed heme oxygenase (Yu *et al.*, 2015; 2016), suggesting that biliverdin concentration is a limiting factor in the fluorescence of these proteins within zebrafish. Other in vitro attempts to augment brightness of bacterial phytochrome-derived FPs included

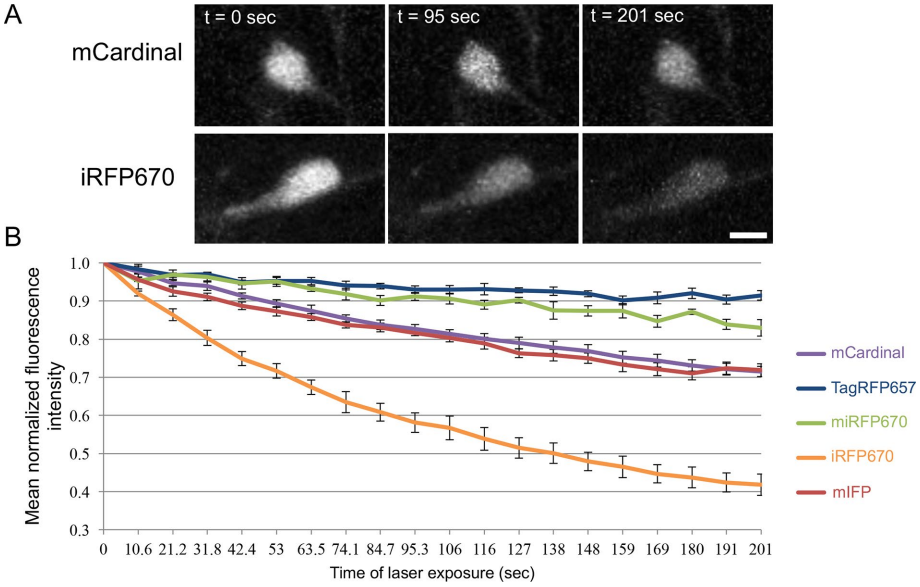

FIGURE 6: Far-red and near-infrared FP photostability. (A) Sample maximum intensity projections (representing depth of 10.76 µm) of cell expressing mCardinal or iRFP670 in hindbrain undergoing bleaching procedure at 70% laser power. Dorsal is up and rostral is to the left. Scale bar represents 5 µm. (B) Quantification of photobleaching shows average normalized fluorescence intensity over time for each FP. TagRFP657 demonstrated the most photostability among near-infrared FPs expressed in the zebrafish hindbrain. Brightness at each time point was normalized by dividing by initial brightness for that FP to show relative proportion of bleaching. Mean normalized brightness value is shown for each time point and error bars represent SEM (mCardinal, TagRFP657, iRFP670: $n = 5$ cells; miRFP670: $n = 6$ cells; mIFP: $n = 4$ cells).

incubation with heme precursor and addition of exogenous biliverdin; these strategies had variable effects on different FPs and, for the most part, had only a weak effect on fluorescence brightness (Shemetov *et al.*, 2017). In our hands, coinjection of heme oxygenase protein had little to no effect on brightness. Primarily, bacterial phytochrome-derived near-infrared FPs were developed for use in mammals, in which biliverdin is ubiquitous, and more red-shifted labels are preferred due to reduced light scattering, autofluorescence, and absorption by hemoglobin and melanin at longer wavelengths (Piatkevich *et al.*, 2013; Marx, 2014; Shcherbakova *et al.*, 2015; Chernov *et al.*, 2017). Though further efforts to increase biliverdin concentration in zebrafish could potentially result in improved brightness for miRFP670, iRFP670, and mIFP, expression of both mCardinal and iRFP670 were sufficiently bright to be imaged alongside Brainbow without the addition of any protein, transgene, or other exogenous molecule. This is preferable because of both the relative ease of expression and the minimal disruption to metabolism. In addition to being the rate-limiting enzyme in an important catabolic pathway among eukaryotes, heme oxygenase is also known to specifically function in zebrafish development (Holowiecki *et al.*, 2017) and cardiac function (Tzaneva and Perry, 2016), and thus its manipulation in zebrafish embryos could potentially confound experimental results. Furthermore, expression of the endogenous zebrafish isoforms of heme oxygenase varies with tissue, sex, and age (Holowiecki *et al.*, 2016), potentially complicating the direct relationship between brightness and FP copy number that allows quantification of fusion protein levels.

Another possible explanation for the discrepancy between the predicted and actual FP brightness is differing degrees of FP expression due to codon optimization. As each organism has a preference for synonymous codons within its genome, known as codon bias, the codon usage of a gene can impact its expression level via numerous mechanisms (reviewed in Plotkin and Kudla, 2011; Quax *et al.*, 2015). A comparison of the codon optimization of the FPs we assessed using the Codon Adaptation Index (CAI) (Sharp and Li, 1987; Puigbò *et al.*, 2008) showed that the GFP-like fluorophores mCardinal and TagRFP657 had a slightly higher degree of codon optimization for expression in zebrafish (CAI values of 0.873 and 0.878, respectively) than the bacteria-derived fluorophores (miRFP670: 0.750, iRFP670: 0.759, mIFP: 0.795; see Table 1). This may have resulted in reduced expression levels of miRFP670, iRFP670, and mIFP, contributing to their apparent dimness. Performance of these FPs may be improved following codon optimization via the substitution of synonymous codons used more frequently in genes highly expressed in zebrafish. This approach, however, has been inconsistently effective in improving gene expression (reviewed in Plotkin and Kudla, 2011; Quax *et al.*, 2015), with some studies finding no correlation between CAI and heterologous protein expression levels (Kudla *et al.*, 2009; Gustafsson *et al.*, 2012). Another possible cause of variable levels of expression among FPs could be variability in Kozak-like sequences upstream of the start codon in DNA constructs encoding these FPs. Small variations in the Kozak consensus sequence have been shown to have significant effects on the translation efficiency of genes in zebrafish, suggesting that applying the most efficient variant of the Kozak sequence in zebrafish could increase the rate of translation and, potentially, the brightness of any of the far-red/near-infrared FPs tested (Grzegorski *et al.*, 2014).

mCardinal as a far-red fluorescent protein for use in zebrafish

Based on our brightness analysis, mCardinal emerges as the superior choice for coexpression studies in zebrafish. In addition to in vivo brightness, we also assessed FP photostability by continuous laser exposure on the confocal microscope. Though mCardinal was not as photostable as TagRFP657 or miRFP670, it nonetheless remained the brightest over time due to its initial superior brightness (Figure 6). Additionally, the photobleaching protocol utilized a laser power of 70%, which is more than seven times higher than necessary for actual imaging of mCardinal to induce sufficient bleaching for quantification and comparison. Under normal acquisition parameters, photobleaching of mCardinal was not observed. Together, these results suggest that mCardinal is suitably photostable for use in developmental studies that require imaging over time. Our results, however, only reflect in vivo bleaching of these FPs under laser excitation; lower intensity illumination from epifluorescence microscopes can induce differential bleaching of FPs, and thus the relative rate of bleaching may vary with imaging system (Shaner *et al.*, 2005). Finally, zebrafish embryos expressing mCardinal did not show signs of cytotoxicity, suggesting that this FP can be used in experiments without harming the cells of interest. While labeling density was not

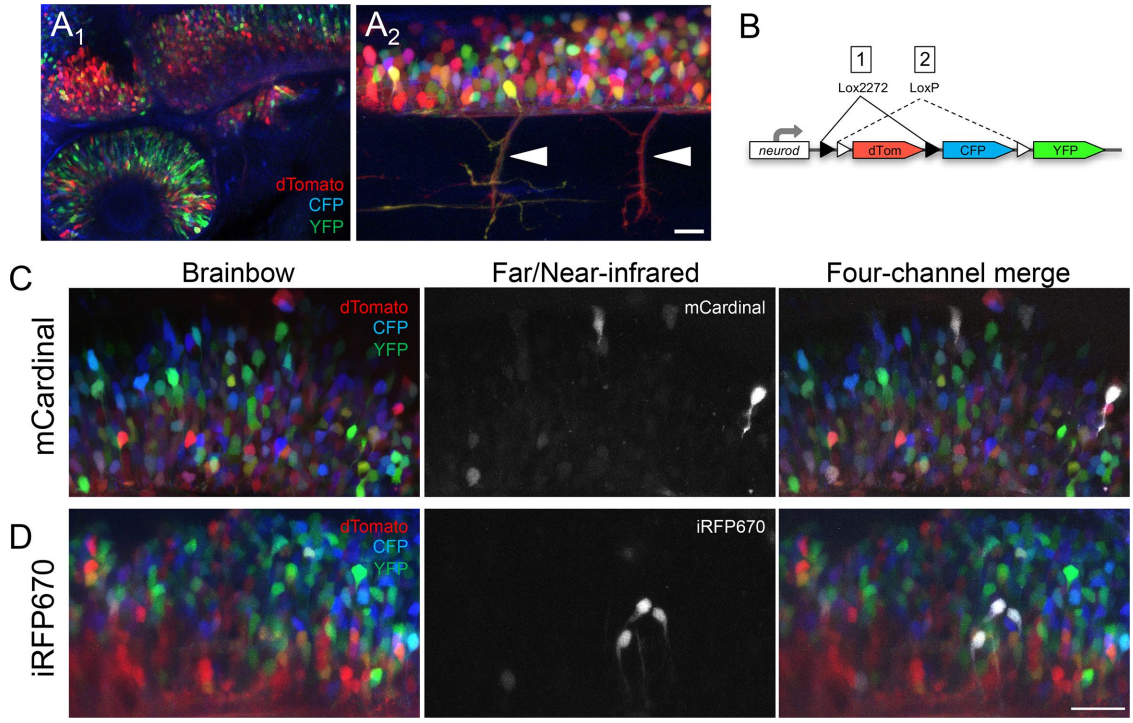

FIGURE 7: In vivo coexpression of far-red/near-infrared FPs in transgenic zebrafish expressing Brainbow. (A1) Tile stitch of *Tg(neurod:Zebrabow)* at 2 dpf. (A2) Spinal cord at 2 dpf. Motor axons denoted by arrowheads. (B) Schematic of neurod:Zebrabow DNA. (C) Maximum intensity projection of hindbrain of 2 dpf *Tg(neurod:Zebrabow)* zebrafish injected with hsp:mCardinal, representing 16 slices for a depth of 13.58 µm. Left panel shows three-channel Brainbow expression, middle shows mCardinal expression, and right shows four-channel merge, with mCardinal displayed as white. Collection range for dTomato set to 566–583 nm. (D) Similar to C but showing hsp:iRFP670 expression in 2 dpf *Tg(neurod:Zebrabow)* zebrafish, projection depth of 20.03 µm. Collection range for dTomato set to 567–621 nm. In all panels, dorsal is up and rostral is to the left. Brightness has been linearly adjusted for display. In A only, nonlinear adjustments were made to display diverse labeling across cell types. Scale bars represent 40 µm in A1; 15 µm in A2; and 25 µm in C and D.

quantitatively compared among FPs, we observed that fish expressing mCardinal frequently had a much higher density of cells labeled than fish expressing other far-red or near-infrared FPs. The consistent survival of a large number of healthy cells that were bright enough to be imaged further suggests that mCardinal is expressed robustly in zebrafish cells and does not impact cellular health.

While mCardinal provided the brightest expression in our hands, and was clearly visualized in the Brainbow context, there may be certain advantages to selecting a near-infrared protein such as iRFP670 for some multicolor studies. Bacterial phytochrome-derived near-infrared FPs are particularly useful because the biliverdin chromophore allows for even further red-shifted spectral absorbance and emission as compared with the non-phytochrome-derived, far-red FPs (reviewed in Shcherbakova *et al.*, 2015). Since the excitation of iRFP670 (peak 643 nm) is significantly red-shifted from both mCardinal (peak 604 nm) and dTomato (peak 554 nm), this means that iRFP670 can be used with little to no concern of bleedthrough with any of the Brainbow FPs. Additionally, the more extreme longer wavelength light may be preferable for deep tissue or even whole-body imaging studies (Ntziachristos *et al.*, 2003; Deliolanis *et al.*, 2008). While mCardinal is also red shifted, it has a broad excitation peak that spans the excitation peak of dTomato (Supplemental Figure 2). This means that care needs to be taken when imaging dTomato and mCardinal together. It is straightforward to excite and unambiguously detect mCardinal in this context; using a laser of ~585 nm or higher will exclude any signal from dTomato as well as from the other Brainbow FPs. However, excitation of Brainbow's dTomato at 561 nm can lead to some inadvertent, off-peak excitation of mCardinal. This means that the signal detected for dTomato may also include dim bleedthrough from mCardinal. Importantly, this bleedthrough from mCardinal can be essentially eliminated by selecting a narrow collection window for dTomato (Supplemental Figure 2). This concern would also be reduced by the use of an excitation laser for dTomato below ~540 nm or the use of a Brainbow construct or other multicolor approach that does not utilize dTomato. Antibody staining can also be used for the dTomato epitope, which is distinct from CFP and YFP since it derives from *Discosoma* as opposed to *Aequorea victoria*. This could amplify the dTomato signal and/or allow it to be detected in a different range. In summary, although there is minimal mCardinal overlap with dTomato, this can be eliminated by the use of careful image acquisition parameters. Importantly, the overlap is in only one direction; there is no contamination from any Brainbow signal when imaging mCardinal, which means that a tagged protein can be unambiguously identified.

Tagging proteins with a fourth color beyond Brainbow for advanced labeling strategies

Our quantitative assessment of FP expression in zebrafish embryos demonstrates that mCardinal has bright and stable expression in a variety of cell types and thus can be utilized as an experimental tool in this useful model organism (Figure 1A). The near-infrared FP iRFP670 did not fluoresce as brightly as mCardinal, but it is also sufficiently bright for imaging in developing zebrafish. Our results also

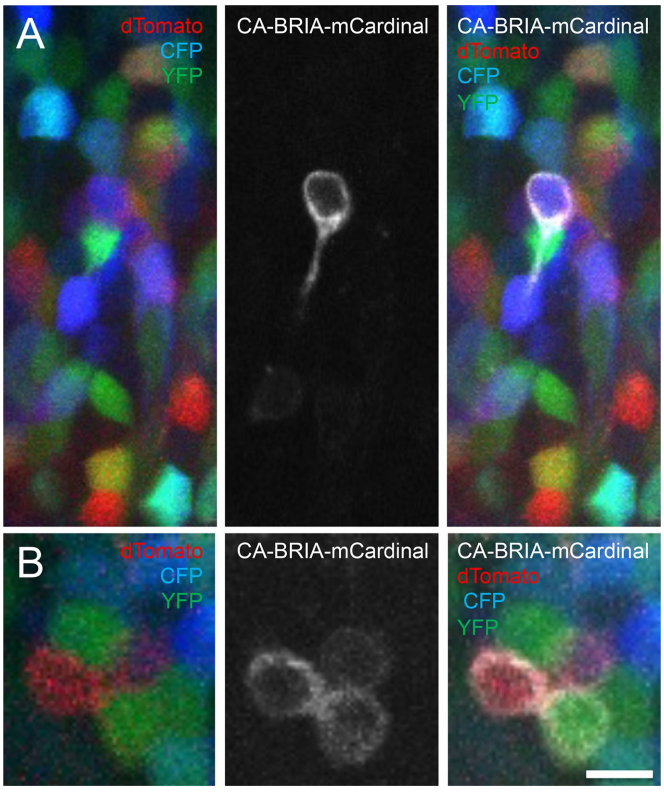

FIGURE 8: In vivo coexpression of manipulated BMP receptor tagged with mCardinal in hindbrain of transgenic Brainbow zebrafish. (A) Maximum intensity projection of 2 dpf *Tg(neurod:Zebrabow)* zebrafish injected with hsp:CA-BRIA-mCardinal, representing eight slices for a depth of 6.79 µm. Left panel shows three-channel Brainbow expression, middle panel shows CA-BRIA-mCardinal expression, and right panel shows four-channel merge, with mCardinal displayed as white. (B) Maximum intensity projection of hindbrain, representing five slices for a depth of 4.24 µm. Scale bar represents 6 µm in A and 5 µm in B. Collection range for dTomato set to 567–591 nm. Dorsal is up and rostral is to the left. Brightness has been linearly adjusted for display.

identify mCardinal and iRFP670 as useful FPs for use in conjunction with Brainbow. Specific proteins can thus be tagged with mCardinal or other monomeric red-shifted FPs to assess mechanistic effects within a Brainbow-labeled population. Here we demonstrate that a constitutively active, mutated form of the BMP receptor 1A, CA-BRIA (Nikaido *et al.*, 1999), tagged with mCardinal, can be coexpressed and visualized within the membrane of a subset of Brainbow-labeled cells. We achieve this expression in a new transgenic zebrafish line, *Tg*(*neurod:Zebrabow*), a useful tool for studies of the developing nervous system. In these fish, Brainbow expression is spatially restricted via the neuroD promoter (Obholzer *et al.*, 2008), a neuronal basic helix-loop-helix transcription factor that is active early in zebrafish development (Korzh *et al.*, 1998). Expression of mCardinal-tagged CA-BRIA within this context allows for an assessment of how increased BMP signaling influences individual cells and their unmanipulated neighboring cells in the proliferative ventricular zone. This type of an approach more broadly provides a powerful strategy for manipulating and visualizing expression of a specific gene in direct comparison with neighboring, labeled but nonmanipulated cells.

The use of mCardinal as a far-red label can be applied not only to the variety of systems that employ Brainbow techniques in zebrafish (e.g., Gupta and Poss, 2012; Pan *et al.*, 2013; Dirian *et al.*, 2014; Xiong *et al.*, 2015; Chen *et al.*, 2016a,b; Foglia *et al.*, 2016; Furlan *et al.*, 2017) but also to other multicolor fluorescent protein labeling systems (e.g., Boldogkoi *et al.*, 2009; Snippert *et al.*, 2010; Distel *et al.*, 2011; Weber *et al.*, 2011; Malide *et al.*, 2012; Worley *et al.*, 2013; Garcia-Marques *et al.*, 2014; Garcia-Moreno *et al.*, 2014; Nern *et al.*, 2015; Pontes-Quero *et al.*, 2017) to ask complex experimental questions requiring spectrally distinct fluorescent labels that are driven by separate promoters. To our knowledge, this is the first example of coexpression of a far-red or near-infrared protein alongside Brainbow and thus demonstrates how red-shifted fluorescent proteins can be used to complement and expand the multicolor technique. This combinatorial approach should be applicable to any of the model organisms in which Brainbow or other multicolor approaches have been used.

MATERIALS AND METHODS

Generation of DNA constructs

DNA constructs for expression in zebrafish were generated using Version D of the MultiSite Gateway Three-Fragment Vector Construction Kit (ThermoFisher Scientific, Waltham, MA). The following plasmids were used as templates: mCardinal-C1 (Michael Davidson, Florida State University; Addgene plasmid #54799), pTagRFP657-C1 (Vladislav Verkhusha, Albert Einstein College of Medicine; Addgene plasmid #31872), pmiRFP670-N1 (Vladislav Verkhusha; Addgene plasmid #79987), piRFP670-N1 (Vladislav Verkhusha; Addgene plasmid #45457), mIFP-N1 (Michael Davidson and Xiaokun Shu, University of California, San Francisco; Addgene plasmid #54620), and pzCA-BRIA/pSP (generous gift from Naoto Ueno, National Institute for Basic Biology). The primers in Table 2 were used for amplification of each gene via PCR while also adding *attB* sites (in bold) to allow for Gateway recombination of the products.

PCR products were recombined with pDONR221 to produce middle entry clones. Middle entry clones containing far-red/near-infrared FP genes were recombined with the following plasmids from the Tol2kit (Kwan *et al.*, 2007): pDESTTol2CG containing cmlc2:EGFP transgenesis marker; p5E-hsp70 containing a zebrafish promoter for heat-shock induction; and p3E-polyA containing an SV40 late polyA signal. In generating an mCardinal-tagged form of CA-BRIA, mCardinal was moved to the 3′ position. To amplify mCardinal from mCardinal-C1 and add *attB* sites suitable for recombination into a 3′ entry clone, the primers in Table 3 were used.

The resultant PCR product was recombined with pDONRP2R-P3 to create p3E-mCardinal. This entry clone was then recombined with pDESTTol2CG containing cmlc2:EGFP transgenesis marker, p5E-hsp70, and pME-CA-BRIA, containing a constitutively active form of the zebrafish BMPR-1A (Q228D; see Nikaido *et al.*, 1999). To ensure that no mutations had arisen in inserts of all entry clones, capillary electrophoresis DNA sequencing was performed in the OHSU DNA Services Core (see *Acknowledgments*).

Zebrafish care and transient gene expression

All protocols involving zebrafish were approved by the Lewis and Clark Institutional Animal Care and Use Committee. Adult wild-type zebrafish (*D. rerio;* AB/TL; Westerfield, 2000; Zebrafish International Resource Center, Eugene, OR) were maintained in a controlled, multitank aquatic housing system (Aquaneering, San Diego, CA) at 27°C in reverse osmosis (RO) water dosed for pH and salinity control. Injected embryos and larvae were maintained in an incubator (Forma Scientific, Marietta, OH) at 28°C in 90 mm petri dishes (Genesee Scientific, San Diego, CA) containing E3 embryo medium (5 mM NaCl [J.T. Baker, Philipsburg, NJ],

Plasmid	Forward primer (attB1)	Reverse primer (attB2)
mCardinal-C1	**GGGG ACA AGT TTG TAC AAA AAA GCA GGC TAT** ATG GTG AGC AAG GGC GAG	**GGGG AC CAC TTT GTA CAA GAA AGC TGG GTA** TTA TCT AGA TCC GGT GGA
pTagRFP657-C1	**GGGG ACA AGT TTG TAC AAA AAA GCA GGC TAT** ATG GTG TCT AAG GGC GAA GA	**GGGG AC CAC TTT GTA CAA GAA AGC TGG GTA** TTA TCT AGA TCC GGT GGA
pmiRFP670-N1	**GGGG ACA AGT TTG TAC AAA AAA GCA GGC TGT** ATG GTA GCA GGT CAT GCC TCT GGC A	**GGGG AC CAC TTT GTA CAA GAA AGC TGG GTT** GCT CTC AAG CGC GGT GAT
piRFP670-N1	**GGGG ACA AGT TTG TAC AAA AAA GCA GGC TCT** ATG GCG CGT AAG GTC GAT C	**GGGG AC CAC TTT GTA CAA GAA AGC TGG GTA** TTA GCG TTG GTG GTG GGC GGC
mIFP-N1	**GGGG ACA AGT TTG TAC AAA AAA GCA GGC TTT** ATG TCG GTA CCG CTG ACT	**GGGG AC CAC TTT GTA CAA GAA AGC TGG GTT** TCA TTT GGA CTG AGA CTG
pzCA-BRIA/pSP	**GGGG ACA AGT TTG TAC AAA AAA GCA GGC TGG** ATG CGT CAG CTT TTG TT C	**GGGG AC CAC TTT GTA CAA GAA AGC TGG GTN** GAT TTT AAT GTC TTG AGA TTC

TABLE 2: Primers used to generate middle entry clones.

0.17 mM KCl [AMRESCO], 0.33 mM $CaCl_2$, 0.33 mM $MgSO_4$ [Sigma, St. Louis, MO], and 0.00001% methylene blue [Sigma]; Nusslein-Volhard and Dahm, 2002) with 0.2 mM phenylthiourea (PTU; Alfa Aesar, Ward Hill, MA) added at 1 dpf to prevent pigmentation.

Brief pulses of air (World Precision Instruments, Sarasota, FL) were used to inject DNA solution from a glass capillary (World Precision Instruments; item TW100F-4) pulled on a micropipette puller (Sutter Instrument Company, Novato, CA) into the yolk of one-cell-stage wild-type AB/TL embryos within 30 min of fertilization. DNA injection solution contained 7.5–10 ng/µl for pEXP-*hsp70*:CA-BRIA-mCardinal, 5% phenol red, and 0.065–0.08 mM KCl. Approximately 4.19 nl of this solution was injected into each embryo, equivalent to 31.4–41.9 pg plasmid DNA for far-red/near-infrared FP constructs and 0.0629 ng for pEXP-*hsp70*:CA-BRIA-mCardinal. To induce transgene expression via the heat-shock promoter, embryos expressing the cmlc2:EGFP marker underwent heat shock in a water bath at 37°C for 80–90 min at 48–52 hpf. Since phytochrome-derived FPs utilize biliverdin as a chromophore, recombinant human heme oxygenase (HO-1; Novus Biologicals, Littleton, CO), which produces biliverdin from heme, was added to the mIFP injection solution at a concentration of 88 or 132 ng/µl, which correlates to roughly 0.369–0.578 ng protein per embryo, in an attempt to increase brightness. For coexpression with Brainbow, DNA constructs (hsp:CA-BRIA-mCardinal, hsp:mCardinal, or hsp:iRFP670) were injected into embryos from *Tg(neurod:Zebrabow)* crossed to *Tg(hsp:Cre^{a134})* fish (Pan *et al.,* 2013).

Generation of stable transgenic zebrafish line

Plasmid DNA for the *Tg(neurod:Zebrabow-polyA)* line, referred to as *Tg(neurod:Zebrabow*), was generated as above, using Gateway Cloning (Invitrogen) and the Tol2kit (Kwan *et al.,* 2007). The Zebrabow cassette was amplified from ubi:Zebrabow (Pan *et al.,* 2013), a gift from Y. A. Pan (Virginia Tech Carilion School of Medicine), using the primers in Table 4. Zebrabow was originally generated from Brainbow (version 1.0), line L (Livet *et al.,* 2007), and contains dTomato as the default color, which can change on Cre-mediated recombination to either mCerulean (referred to here as CFP) or EYFP (referred to here as YFP; see construct in Figure 7B).

The PCR product was combined with pDONR221 to generate pME-Zebrabow. An LR reaction was then performed using p5E-neurod (gift from T. Nicolson, Stanford University) pME-Zebrabow, p3E-polyA, and pDestTol2CG2 to generate *neurod:Zebrabow-polyA*.

To generate the transgenic line, capped mRNA was generated from pCS2FA Transposase using the T7 mMessage mMachine in vitro synthesis kit (Life Technologies AM1344). Approximately 12.9 pg/embryo (50 ng/µl in the injection mix) each of *neurod:Zebrabow* and transposase mRNA were injected into one-cell-stage wild-type AB/TL zebrafish embryos. F1 progeny from potential founders were screened for dTomato expression, raised to adulthood, and outcrossed to wild-type AB/TL fish. To initiate Brainbow recombination in embryos, *Tg(neurod:Zebrabow*) zebrafish were crossed to *Tg(hsp:Cre^{a134})* (Pan *et al.,* 2013) and then embryos underwent heat shock in a water bath at 37°C for ~90 min at 24–26 hpf. Some fish expressing Brainbow (and not used for FP brightness quantification) underwent a second heat shock at 48–51 hpf, prior to imaging.

Live imaging

For live imaging experiments, zebrafish at 50–55 hpf were anesthetized in ~0.2 mM MS-222 Tricaine-S (Western Chemical, Ferndale, WA) diluted in E3 medium and then mounted in 1% low-melt agarose (Agarose SFR; AMRESCO, Solon, OH). Cells within the

Forward primer (attB2)	Reverse primer (attB3)
GGGG ACA GCT TTC TTG TAC AAA GTG GGA ATG GTG AGC AAG GGC GAG	**GGGG AC AAC TTT GTA TAA TAA AGT TGT** TAC TTG TAC AGC TCG TCC ATG CCA TTA

TABLE 3: Primers used to generate 3′ entry clone for mCardinal.

Forward primer (attB1): Zebrabow	Reverse primer (attB2): Zebrabow
GGGG ACA AGT TTG TAC AAA AAA GCA GGC TGC GAG CTC ATA ACT TCG TAT	**GGGG AC CAC TTT GTA CAA GAA AGC TGG GTG** CAG ATC ACG CGT ATT AC

TABLE 4: Primers used to amplify Zebrabow.

zebrafish hindbrain as well as muscle cells were targeted for imaging. All imaging was performed on a laser-scanning confocal microscope (Carl Zeiss LSM 710, Oberkochen, Germany), using a Zeiss 20X (1.0 NA) water immersion objective with an additional zoom of 1.5, except the mCardinal whole fish tile stitch (Figure 1), which was taken using a Zeiss 10X (0.3 NA) objective, and the *neurod:Zebrabow* (Figure 7), which was done using a zoom of 1.5.

Far-red and near-infrared FPs were imaged using a HeNe633 laser, a 458/514/561/633 main beam splitter, and a broad collection range of 638–747 nm to maximize brightness. For three-channel Brainbow imaging, a DPSS 561 laser was used to excite dTomato, an argon laser was used to excite CFP (mCerulean) at 458 nm, and YFP (EYFP) at 514 nm. Each FP channel was imaged sequentially by frame, except for some images where CFP and dTomato were imaged simultaneously. Collection ranges for Brainbow were set to 463–521 nm for CFP, 519–555 nm for YFP, and 567–591 nm for dTomato, unless otherwise noted in figure legends. For four-channel image acquisition, CFP and either mCardinal or iRFP670 were imaged simultaneously, while YFP and dTomato were each imaged sequentially by frame. For four-channel Brainbow imaging, mCardinal or iRFP670 collection was expanded to 638–758 nm, and when imaging with mCardinal, Brainbow settings were optimized by decreasing the dTomato collection range to 566–583 nm. Images were acquired using Zen Black software (Carl Zeiss, Oberkochen, Germany), saved as .czi files, and subsequently imported into Fiji software (Schindelin *et al.,* 2012) using the BioFormats Importer (The Open Microscopy Environment). For on-screen display, the dTomato channel was coded as red, the YFP channel was coded as green, and the CFP channel was coded as blue. Since far-red/near-infrared FPs emit in a nonvisible range, it was digitally coded in grayscale for on-screen viewing.

For photobleaching experiments, bright neurons in the hindbrain were selected. A rectangular region of interest (~28 × 28 µm) was drawn encompassing the cell and 20 cycles of small Z-stacks (10.76 µm) were collected with a pixel dwell time of 1.58 µs and interval of 0 ms to standardize scanning time. Laser power was increased to 70% to induce appreciable bleaching. For some experiments, Z-stacks of the entire field were taken before and after the photobleaching experiment to rule out drift in cells of interest.

Analysis

Data on excitation and emission spectra were collected from spectra published in Morozova *et al.* (2010), Chu *et al.* (2014), Shcherbakova *et al.* (2016), Shcherbakova and Verkhusha (2013), and Yu *et al.* (2016) using WebPlotDigitizer software; normalized fluorescence values were taken at nanometer increments as described in Heppert *et al.* (2016). Predicted brightness was calculated by multiplying the fraction of a FP's emission peak within the collection range by the FP's brightness at the excitation wavelength used. The fraction of the total emission within the collection range was calculated by dividing the sum of the normalized emission values for 638–747 nm by the total sum of the normalized emission values. The brightness at the excitation wavelength was calculated by multiplying the quantum yield, the extinction coefficient (as reported in Morozova *et al.*, 2010; Chu *et al.*, 2014; Shcherbakova *et al.*, 2016; Shcherbakova and Verkhusha, 2013; and Yu *et al.*, 2015), and the normalized excitation value at 633 nm. Predicted brightness when using a 647-nm laser line was also calculated in the same manner, using the fraction of the emission peak within a collection range of 652–761 nm and the normalized excitation value at 647 nm.

Actual brightness was quantified using the Fiji software (Schindelin *et al.,* 2012) using the elliptical tool to select the cell body in the central focal plane (hindbrain cells) or the rectangular tool to select the largest continuous area of cell body visible in a single focal plane (muscle cells). Background intensity was calculated for each section of a Z-stack by averaging three rectangular selections within the fish where no cells were visible. The raw fluorescence values from each section were then normalized by subtracting the corresponding mean background value. For optimal viewing but also comparable image presentation of far-red and near-infrared FPs in figures, linear image adjustments were made to images. These adjustments were identical for comparison across FPs. For example, in Figures 2, 3, and 4A, the maximum brightness level of each image was adjusted to 350. In Figure 6, brightness of cells at $t = 0$ were normalized to each other for displaying photobleaching.

Photobleaching effects were quantified using the Fiji software. Maximum intensity projections of the small Z-stack (one cell thick) were generated for each time point; in these projections, the freehand tool was used to select the cell body. Measurements of the same ROI were taken at each time point and brightness values were normalized by dividing by the initial brightness.

Fluorescence normalization was performed in Google Sheets while all other data analysis was performed in R: A Language and Environment for Statistical Computing (Vienna, Austria; R Core Team, 2017). First, mean cell brightness was calculated for each fish used in brightness comparisons. These values were then averaged to find a mean brightness for each FP condition; SEM was also calculated to describe variation in these groups. Linear modeling was used to determine whether mean cell brightness per fish varied significantly between FP conditions, while Tukey's post hoc test was used to perform pairwise comparisons between FPs. All statistical analysis was performed separately for hindbrain and muscle data. CAI values were calculated using the CAIcal server (Puigbò *et al.,* 2008) with the codon usage reference table for *D. rerio* from the Codon Usage Database (Nakamura *et al.,* 2000).

ACKNOWLEDGMENTS

We thank Michael Davidson for creating and distributing mCardinal; Xiaokun Shu (and Michael Davidson) for mIFP; Vladislav Verkhusha for TagRFP657, miRFP670, and iRFP670; Naoto Ueno for CA-BRIA; Albert Pan for Zebrabow DNA and *Tg(hsp:Cre)* fish; Kara Cerveny for help generating transposase RNA, for sharing embryos, and for helpful discussions; Teresa Nicolson for p5E-neurod; Alex Nechiporuk for sharing Gateway reagents; K. M. Carey for zebrafish maintenance and mating; and M. Metz, P. A. Zobel-Thropp, Greta Glover, and V. Unni for helpful discussions. The OHSU DNA Services Core uses a 3730xl DNA Analyzer that was purchased with funding from National Institutes of Health SIG grant S10 OD010609. This work was supported by National Science Foundation Award 1553764, the M.J. Murdock Charitable Trust, and the John S. Rogers Research Program at Lewis and Clark College.

REFERENCES

Albadri S, De Santis F, Di Donato V, Del Bene F (2017). CRISPR/Cas9-mediated knockin and knockout in zebrafish. In: Genome Editing in Neurosciences. Research and Perspectives in Neurosciences, ed. R Jaenisch, F Zhang, and F Gage, Cham, Switzerland: Springer.

Alon A, Schmidt HR, Wood MD, Sahn JJ, Martin SF, Kruse AC (2017). Identification of the gene that codes for the σ2 receptor. Proc Natl Acad Sci USA 114, 7160–7165.

Ando K, Fukuhara S, Izumi N, Nakajima H, Fukui H, Kelsh RN, Mochizuki N (2016). Clarification of mural cell coverage of vascular endothelial cells by live imaging of zebrafish. Development 143, 1328–1339.

Ansari AM, Ahmed AK, Matsangos AE, Lay F, Born LJ, Marti G, Harmon JW, Sun Z (2016). Cellular GFP toxicity and immunogenicity: potential confounders in in vivo cell tracking experiments. Stem Cell Rev 12, 553–559.

Auldridge M, Forest K (2011). Bacterial phytochromes: more than meets the light. Crit Rev Biochem Mol Biol 46, 67–88.

Avagyan S, Henninger JE, Moore J, Mannherz W, Zon LI (2016). Modeling clonal hematopoietic disorders in zebrafish using color barcoding. Blood 128, 3147.

Bellini D, Papiz MZ (2012). Structure of a bacteriophytochrome and light-stimulated protomer swapping with a gene repressor. Structure 20, 1436–1446.

Bergeron AC, Seman BG, Hammond JH, Archambault LS, Hogan DA, Wheeler RT (2017). Candida and Pseudomonas interact to enhance virulence of mucosal infection in transparent zebrafish. Infect Immun 85, e00475–17.

Bertolin G, Sizaire F, Herbomel G, Reboutier D, Prigent C, Tramier M (2016). A FRET biosensor reveals spatiotemporal activation and functions of aurora kinase A in living cells. Nature Commun 7, 12674.

Boldogkoi Z, Balint K, Awatramani GB, Balya D, Busskamp V, Viney TJ, Lagali SP, Duebel J, Pásti E, Tombácz D, *et al*. (2009). Genetically timed, activity-sensor and rainbow transsynaptic viral tools. Nat Methods 6, 127–130.

Bubnell J, Pfister P, Sapar ML, Rogers ME, Feinstein P (2013). β2 Adrenergic receptor fluorescent protein fusions traffic to the plasma membrane and retain functionality. PLoS One 8, e74941.

Cai D, Cohen KB, Luo T, Lichtman JW, Sanes JR (2013). Improved tools for the Brainbow toolbox. Nat Methods 10, 540.

Chen A, Chiu CN, Mosser EA, Kahn S, Spence R, Prober DA (2016a). QRFP and its receptors regulate locomotor activity and sleep in zebrafish. J Neurosci 36, 1823–1840.

Chen C, Puliafito A, Cox B, Primo L, Fang Y, Di Talia S, Poss K (2016b). Multicolor cell barcoding technology for long-term surveillance of epithelial regeneration in zebrafish. Dev Cell 36, 668–680.

Chernov KG, Redchuk TA, Omelina ES, Verkhusha VV (2017). Near-infrared fluorescent proteins, biosensors, and optogenetic tools engineered from phytochromes. Chem Rev 117, 6423–6446.

Choi JH, Sim SE, Kim JI, Choi DI, Oh J, Ye S, Lee J, Kim T, Ko HG, Lim CS, Kaang BK (2018). Interregional synaptic maps among engram cells underlie memory formation. Science 360, 430–435.

Chu J, Haynes R, Corbel S, Li P, González-González E, Burg J, Ataie N, Lam A, Cranfill P, Baird M, *et al*. (2014). Non-invasive intravital imaging of cellular differentiation with a bright red-excitable fluorescent protein. Nat Methods 11, 572–578.

Cid E, Yamamoto M, Buschbeck M, Yamamoto F (2013). Murine cell glycolipids customization by modular expression of glycosyltransferases. PLoS One 8, e64728.

Day R, Davidson M (2009). The fluorescent protein palette: tools for cellular imaging. Chem Soc Rev 38, 2887–2921.

Deliolanis NC, Kasmieh R, Würdinger T, Tannous BA, Shah K, Ntziachristos V (2008). Performance of the red-shifted fluorescent proteins in deep-tissue molecular imaging applications. J Biomed Opt 13, 044008.

Dirian L, Galant S, Coolen M, Chen W, Bedu S, Houart C, Bally-Cuif L, Foucher I (2014). Spatial regionalization and heterochrony in the formation of adult pallial neural stem cells. Dev Cell 30, 123–136.

Distel M, Hocking J, Koster R (2011). In vivo cell biology using Gal4-mediated multicolor sub cellular labeling in zebrafish. Commun Integr Biol 4, 336–339.

Dovrat D, Dahan D, Sherman S, Tsirkas I, Elia N, Aharoni, A (2018). A live-cell imaging approach for measuring DNA replication rates. Cell Rep 24, 252–258.

Dunsing V, Mayer M, Liebsch F, Multhaup G, Chiantia S (2017). Direct evidence of amyloid precursor-like protein 1 trans interactions in cell–cell adhesion platforms investigated via fluorescence fluctuation spectroscopy. Mol Biol Cell, 28, 3609–3620.

Egawa T, Hanaoka K, Koide Y, Ujita S, Takahashi N, Ikegaya Y, Matsuki N, Terai T, Ueno T, Komatsu T, Nagano T (2011). Development of a far-red to near-infrared fluorescence probe for calcium ion and its application to multicolor neuronal imaging. J Am Chem Soc. 133, 14157–14159.

Feng S, Sekine S, Pessino V, Li H, Leonetti MD, Huang B (2017). Improved split fluorescent proteins for endogenous protein labeling. Nat Commun 8, 370.

Filonov GS, Piatkevich KD, Ting L-M, Zhang J, Kim K, Verkhusha VV (2011). Bright and stable near infra-red fluorescent protein for *in vivo* imaging. Nat Biotechnol 29, 757–761.

Filonov GS, Krumholz A, Xia J, Yao J, Wang LV, Verkhusha VV (2012). Deep-tissue photoacoustic tomography of a genetically encoded near-infrared fluorescent probe. Angew Chem Int Ed Engl 51, 1448–1451.

Foglia MJ, Cao J, Tornini VA, Poss KD (2016). Multicolor mapping of the cardiomyocyte proliferation dynamics that construct the atrium. Development 143, 1688–1696.

Furlan G, Cuccioli V, Vuillemin N, Dirian L, Muntasell AJ, Coolen M, Dray N, Bedu S, Houart C, Beaurepaire E, *et al*. (2017). Life-long neurogenic activity of individual neural stem cells and continuous growth establish an outside-in architecture in the teleost pallium. Curr Biol 27, 3288–3301.

Garcia-Marques J, Nunez-Llaves R, Lopez-Mascaraque L (2014). NG2-glia from pallial progenitors produce the largest clonal clusters of the brain: time frame of clonal generation in cortex and olfactory bulb. J Neurosci 34, 2305–2313.

Garcia-Moreno F, Vasistha NA, Begbie J, Molnar Z (2014). CLoNe is a new method to target single progenitors and study their progeny in mouse and chick. Development 141, 1589–1598.

Ghodke H, Caldas VE, Punter CM, van Oijen AM, Robinson A (2016). Single-molecule specific mislocalization of red fluorescent proteins in live *Escherichia coli*. Biophys J 111, 25–27.

Giepmans B, Adams S, Ellisman M, Tsien R (2006). The fluorescent toolbox for assessing protein location and function. Science 312, 217–24.

Giraud E, Fardoux J, Fourrier N, Hannibal L, Genty B, Bouyer P, Dreyfus B, Verméglio A (2002). Bacteriophytochrome controls photosystem synthesis in anoxygenic bacteria. Nature 417, 202–205.

Giraud E, Verméglio A (2008). Bacteriophytochromes in anoxygenic photosynthetic bacteria. Photosynth Res 97, 141.

Grzegorski SJ, Chiari EF, Robbins A, Kish PE, Kahana A (2014). Natural variability of Kozak sequences correlates with function in a zebrafish model. PLoS One 9, e108475.

Gupta T, Marquart GD, Horstick EJ, Tabor KM, Pajevic S, Burgess HA (2018). Morphometric analysis and neuroanatomical mapping of the zebrafish brain. Methods 150, 49–62.

Gupta V, Poss K (2012). Clonally dominant cardiomyocytes direct heart morphogenesis. Nature 484, 479–484.

Gustafsson C, Minshull J, Govindarajan S, Ness J, Villalobos A, Welch M (2012). Engineering genes for predictable protein expression. Protein Expr Purif 83, 37–46.

Halloran MC, Sato-Maeda M, Warren JT, Su F, Lele Z, Krone PH, Kuwada JY, Shoji W (2000). Laser-induced gene expression in specific cells of transgenic zebrafish. Development 127, 1953–1960.

Han P, Bloomekatz J, Ren J, Zhang R, Grinstein JD, Zhao L, Burns CG, Burns CE, Anderson RM, Chi NC, (2016). Coordinating cardiomyocyte interactions to direct ventricular chamber morphogenesis. Nature 534, 700.

Heap L, Goh CC, Kassahn KS, Scott EK (2013). Cerebellar output in zebrafish: an analysis of spatial patterns and topography in eurydendroid cell projections. Front Neural Circuits 7, 53.

Heim R, Prasher D, Tsien R (1994). Wavelength mutations and posttranslational autoxidation of green fluorescent protein. Biochemistry 91, 12501–12504.

Henninger J, Santoso B, Hans S, Durand E, Moore J, Mosimann C, Brand M, Traver D, Zon L (2017). Clonal fate mapping quantifies the number of haematopoietic stem cells that arise during development. Nat Cell Biol 19, 17–27.

Heppert J, Dickinson D, Pani A, Higgins C, Steward A, Ahringer J, Kuhn J, Goldstein B (2016). Comparative assessment of fluorescent proteins for in vivo imaging in an animal model system. Mol Biol Cell 27, 3385–3394.

Herget U, Gutierrez-Triana JA, Thula OS, Knerr B, Ryu S (2017). Single-cell reconstruction of oxytocinergic neurons reveals separate hypophysiotropic and encephalotropic subtypes in larval zebrafish. eNeuro 4, ENEURO.0278-16.2016.

Hirakawa M, Nagakubo D, Kanzler B, Avilov S, Krauth B, Happe C, Swann JB, Nusser A, Boehm T (2018). Fundamental parameters of the developing thymic epithelium in the mouse. Sci Rep 8, 11095.

Holowiecki A, O'Shields B, Jenny MJ (2016). Characterization of heme oxygenase and biliverdin reductase gene expression in zebrafish (*Danio rerio*): Basal expression and response to pro-oxidant exposures. Toxicol Appl Pharmacol 311, 74–87.

Holowiecki A, O'Shields B, Jenny MJ (2017). Spatiotemporal expression and transcriptional regulation of heme oxygenase and biliverdin reductase genes in zebrafish (*Danio rerio*) suggest novel roles during early developmental periods of heightened oxidative stress. Comp Biochem Physiol C Toxicol Pharmacol 191, 138–151.

Katayama H, Yamamoto A, Mizushima N, Yoshimori T, Miyawaki A (2008). GFP-like proteins stably accumulate in lysosomes. Cell Struc Funct 33, 1–12.

Kesavan G, Hammer J, Hans S, Brand M (2018). Targeted knock-in of CreER T2 in zebrafish using CRISPR/Cas9. Cell Tissue Res 372, 41–50.
Kim SE, Jo SD, Kwon KC, Won YY, Lee J (2017). Genetic assembly of double-layered fluorescent protein nanoparticles for cancer targeting and imaging. Adv Sci 4, 1600471.
Kinkhabwala A, Riley M, Koyama M, Monen J, Satou C, Kimura Y, Higashijima SI, Fetcho J (2011). A structural and functional ground plan for neurons in the hindbrain of zebrafish. Proc Natl Acad Sci USA 108, 164–1169.
Kochhan E, Lenard A, Ellertsdottir E, Herwig L, Affolter M, Belting HG, Siekmann AF (2013). Blood flow changes coincide with cellular rearrangements during blood vessel pruning in zebrafish embryos. PloS One 8, e75060.
Ko S, Chen X, Yoon J, Shin I (2011). Zebrafish as a good vertebrate model for molecular imaging using fluorescent probes. Chem Soc Rev 40, 2120–2130.
Korzh V, Sleptsova I, Liao J, He J, Gong Z (1998). Expression of zebrafish bHLH genes ngn1and nrd defines distinct stages of neural differentiation. Dev Dyn 213, 92–104.
Kremers G, Gilbert S, Cranfill P, Davidson M, Piston D (2011). Fluorescent proteins at a glance. J Cell Sci 124, 157–160.
Kudla G, Murray AW, Tollervey D, Plotkin JB (2009). Coding-sequence determinants of gene expression in Escherichia coli. Science 324, 255–258.
Kwan KM, Fujimoto E, Grabher C, Mangum BD, Hardy ME, Campbell DS, Parant JM, Yost HJ, Kanki JP, Chien CB (2007). The Tol2kit: A multisite gateway-based construction kit forTol2 transposon transgenesis constructs. Dev Dyn 236, 3088–3099.
Kyung T, Lee S, Kim JE, Cho T, Park H, Jeong YM, Kim D, Shin A, Kim S, Baek J, Kim J (2015). Optogenetic control of endogenous Ca^{2+} channels in vivo. Nat Biotech 33, 1092.
Lee S, Lim WA, Thorn KS (2013). Improved blue, green, and red fluorescent protein tagging vectors for *S. cerevisiae*. PLoS One 8, e67902.
Lin MZ, McKeown MR, Ng HL, Aguilera TA, Shaner NC, Campbell RE, Adams SR, Gross LA, Ma W, Alber T, Tsien RY (2009). Autofluorescent proteins with excitation in the optical window for intravital imaging in mammals. Chem Biol 16, 1169–1179.
Livet J, Weissman T, Kang H, Draft R, Lu J, Bennis R, Sanes J, Lichtman J (2007). Transgenic strategies for combinatorial expression of fluorescent proteins in the nervous system. Nature 450, 56–62.
Liu W, Shcherbakova DM, Kurupassery N, Li Y, Zhou Q, Verkhusha VV, Yao J (2018). Quad-mode functional and molecular photoacoustic microscopy. Sci Rep 8, 11123.
Loulier K, Barry R, Mahou P, Le Franc Y, Supatto W, Matho KS, Ieng S, Fouquet S, Dupin E, Benosman R, Chédotal A (2014). Multiplex cell and lineage tracking with combinatorial labels. Neuron 81, 505–520.
Maass PG, Barutcu AR, Shechner DM, Weiner CL, Melé M, Rinn JL (2018). Spatiotemporal allele organization by allele-specific CRISPR live-cell imaging (SNP-CLING). Nat Struct Mol Biol 25, 176–184.
Malide D, Metais JY, Dunbar CE (2012). Dynamic clonal analysis of murine hematopoietic stem and progenitor cells marked by 5 fluorescent proteins using confocal and multiphoton microscopy. Blood 120, e105–e116.
Mao YT, Zhu JX, Hanamura K, Iurilli G, Datta SR, Dalva MB (2018). Filopodia conduct target selection in cortical neurons using differences in signal kinetics of a single kinase. Neuron 98, 67–782.
Martin-Lopez E, Ishiguro K, Greer CA (2017). The laminar organization of piriform cortex follows a selective developmental and migratory program established by cell lineage. Cerebral Cortex 1–16.
Marx V (2014). Probes: seeing in the near-infrared. Nat Methods 11, 717–720.
Matz MV, Fradkov AF, Labas YA, Savitsky AP, Zaraisky AG, Markelov ML, Lukyanov SA (1999). Fluorescent proteins from nonbioluminescent Anthozoa species. Nat Biotech 17, 969
Morozova K, Piatkevich K, Gould T, Zhang J, Bewersdorf J, Verkhusha V (2010). Far-red fluorescent protein excitable with red lasers for flow cytometry and superresolution STED nanoscopy. Biophys J 99, L13–L15
Nakamura Y, Gojobori T, Ikemura T (2000). Codon usage tabulated from international DNA sequence databases: status for the year 2000. Nucleic Acids Res 28, 292.
Nern A, Pfeiffer BD, Rubin GM (2015). Optimized tools for multicolor stochastic labeling reveal diverse stereotyped cell arrangements in the fly visual system. Proc Natl Acad Sci USA 112, E2967–E2976
Nikaido M, Tada M, Takeda H, Kuroiwa A, Ueno N (1999). *In vivo* analysis using variants of zebrafish BMPR-IA: range of action and involvement of BMP in ectoderm patterning. Development 126, 181–190.
Ntziachristos V, Bremer C, Weissleder R (2003). Fluorescence imaging with near-infrared light: new technological advances that enable in vivo molecular imaging. Eur Radiol 13, 195–208.
Nusslein-Volhard C, Dahm R (2002). Zebrafish, Oxford, UK: Oxford University Press.
Obholzer N, Wolfson S, Trapani JG, Mo W, Nechiporuk A, Busch-Nentwich E, Seiler C, Sidi S, Söllner C, Duncan RN, *et al*. (2008). Vesicular glutamate transporter 3 is required for synaptic transmission in zebrafish hair cells. J Neurosci 28, 2110–2118.
Pagán AJ, Yang CT, Cameron J, Swaim LE, Ellett F, Lieschke GJ, Ramakrishnan L (2015). Myeloid growth factors promote resistance to mycobacterial infection by curtailing granuloma necrosis through macrophage replenishment. Cell Host Microbe 18, 15–26.
Pan YA, Livet J, Sanes JR, Lichtman JW, Schier AF (2011). Multicolor Brainbow imaging in zebrafish. Cold Spring Harb Protoc 2011, pdb.prot5546.
Pan YA, Freundlich T, Weissman TA, Schoppik D, Wang XC, Zimmerman S, Ciruna B, Sanes JR, Lichtman JW, Schier AF (2013). Zebrabow: multispectral cell labeling for cell tracing and lineage analysis in zebrafish. Development 140, 2835–2846
Park K, Jeong J, Chung BH (2014). Live imaging of cellular dynamics using a multi-imaging vector in single cells. Chem Commun 50, 10734–10736.
Piatkevich KD, Subach FV, Verkhusha VV (2013). Engineering of bacterial phytochromes for near-infrared imaging, sensing, and light-control in mammals. Chem Soc Rev 42, 3441–3452.
Piatkevich KD, Suk HJ, Kodandaramaiah SB, Yoshida F, DeGennaro EM, Drobizhev M, Hughes TE, Desimone R, Boyden ES, Verkhusha VV (2017). Near-infrared fluorescent proteins engineered from bacterial phytochromes in neuroimaging. Biophys J 113, 2299–2309.
Plotkin JB, Kudla G (2011). Synonymous but not the same: the causes and consequences of codon bias. Nat Rev Genet 12, 32.
Pontes-Quero S, Heredia L, Casquero-García V, Fernández-Chacón M, Luo W, Hermoso A, Bansal M, Garcia-Gonzalez I, Sanchez-Muñoz MS, Perea JR, *et al*. (2017). Dual ifgMosaic: a versatile method for multispectral and combinatorial mosaic gene-function analysis. Cell 170, 800–814.
Puigbò P, Bravo IG, Garcia-Vallve S (2008). CAIcal: a combined set of tools to assess codon usage adaptation. Biol Direct 3, 38.
Quax TE, Claassens NJ, Söll D, van der Oost J (2015). Codon bias as a means to fine-tune gene expression. Mol Cell 59, 149–161.
R Core Team (2017). R: A language and environment for statistical computing. R Foundation for Statistical Computing, Vienna, Austria. www.R-project.org/.
Rice WL, Shcherbakova DM, Verkhusha VV, Kumar AT (2015). *In vivo* tomographic imaging of deep seated cancer using fluorescence lifetime contrast. J Cancer Res 75, 1236–1243.
Robles E, Filosa A, Baier H (2013). Precise lamination of retinal axons generates multiple parallel input pathways in the tectum. J Neurosci 33, 5027–5039.
Rockwell N, Su Y, Lagarias J (2006). Phytochrome structure and signaling mechanisms. Annu Rev Plant Biol 57, 837–858.
Rodriguez E, Campbell R, Lin J, Lin M, Miyawaki A, Palmer A, Shu X, Zhang J, Tsien R (2017). The growing and glowing toolbox of fluorescent and photoactive proteins. Trends Biochem Sci 42, 111–129.
Sapar ML, Ji H, Wang B, Poe AR, Dubey K, Ren X, Ni JQ, Han C (2018). Phosphatidylserine externalization results from and causes neurite degeneration in Drosophila. Cell Rep 24, 2273–2286.
Scheer H, Zhao K (2008). Biliprotein maturation: the chromophore attachment. Mol Microbiol 68, 263–276.
Schindelin J, Arganda-Carreras I, Frise E, Kaynig V, Longair M, Pietzsch T, Preibisch S, Rueden C, Saalfeld S, Schmid B, Tinevez JY (2012). Fiji: an open-source platform for biological-image analysis. Nat Methods 9, 676–682.
Shaner N, Steinbach P, Tsien R (2005). A guide to choosing fluorescent proteins. Nat Methods 2, 905–909.
Sharp PM, Li WH (1987). The codon adaptation index-a measure of directional synonymous codon usage bias, and its potential applications. Nucleic Acids Res 15, 1281–1295.
Shcherbakova D, Verkhusha V (2013). Near-infrared fluorescent proteins for multicolor *in vivo* imaging. Nat Methods 10, 751–754.
Shcherbakova D, Baloban M, Verkhusha V (2015). Near-infrared fluorescent proteins engineered from bacterial phytochromes. Curr Opin Chem Biol 27, 52–63.
Shcherbakova D, Baloban M, Emelyanov A, Brenowitz M, Guo P, Verkhusha V (2016). Bright monomeric near-infrared fluorescent proteins as tags and biosensors for multiscale imaging. Nat Commun 7, 12405.
Shcherbo D, Merzlyak EM, Chepurnykh TV, Fradkov AF, Ermakova GV, Solovieva EA, Lukyanov KA, Bogdanova EA, Zaraisky AG, Lukyanov S,

Chudakov DM (2007). Bright far-red fluorescent protein for whole-body imaging. Nat Methods 4, 741–745
Shemetov AA, Oliinyk OS, Verkhusha VV (2017). How to increase brightness of near-infrared fluorescent proteins in mammalian cells. Cell Chem Biol 24, 758–766.
Shemiakina II, Ermakova GV, Cranfill PJ, Baird MA, Evans RA, Souslova EA, Staroverov DB, Gorokhovatsky AY, Putintseva EV, Gorodnicheva TV, Chepurnykh TV (2012). A monomeric red fluorescent protein with low cytotoxicity. Nat Commun 3, 1204.
Shimomura O, Johnson F, Saiga Y (1962). Extraction, purification and properties of aequorin, a bioluminescent protein from the luminous hydromedusan, Aequorea. J Cell Comp Physiol 59, 223–239.
Shimomura O (2005). The discovery of green fluorescent protein. J Microsc 217, 3–15.
Shoji W, Sato-Maeda M (2008). Application of heat shock promoter in transgenic zebrafish. Dev Growth Differ 50, 401–406.
Singh SP, Janjuha S, Hartmann T, Kayisoglu Ö, Konantz J, Birke S, Murawala P, Alfar EA, Murata K, Eugster A, Tsuji N (2017). Different developmental histories of beta-cells generate functional and proliferative heterogeneity during islet growth. Nat Commun 8, 664.
Snippert HJ, van der Flier LG, Sato T, van Es JH, van den Born M (2010). Intestinal crypt homeostasis results from neutral competition between symmetrically dividing Lgr5 stem cells. Cell 143, 134–144.
Stuart GW, McMurray JV, Westerfield M (1988). Replication, integration and stable germ-line transmission of foreign sequences injected into early zebrafish embryos. Development 103, 403–412.
Stuart GW, Vielkind JR, McMurray JV, Westerfield M (1990). Stable lines of transgenic zebrafish exhibit reproducible patterns of transgene expression. Development 109, 577–584.
Syga Ł, Spakman D, Punter CM, Poolman B (2018). Method for immobilization of living and synthetic cells for high-resolution imaging and single-particle tracking. Sci Rep 8, 13789.
Telford WG, Shcherbakova DM, Buschke D, Hawley TS, Verkhusha VV (2015). Multiparametric flow cytometry using near-infrared fluorescent proteins engineered from bacterial phytochromes. PLoS One 10, e0122342.
Toseland C (2013). Fluorescent labeling and modification of proteins. J Chem Biol 6, 85–95.
Tzaneva V, Perry S (2016). Evidence for a role of heme oxygenase-1 in the control of cardiac function in zebrafish (*Danio rerio*) exposed to hypoxia. J Exp Biol 219, 1563–1571.
Wan G, Fields B, Spracklin G, Phillips C, Kennedy S (2017). Transgenerational epigenetic inheritance factors localize to spatially and temporally ordered liquid droplet assemblages. bioRxiv 220111.
Weber K, Thomaschewski M, Warlich M, Volz T, Cornils K, Niebuhr B, Täger M, Lütgehetmann M, Pollok JM, Stocking C, *et al*. (2011). RGB marking facilitates multicolor clonal cell tracking. Nat Med 17, 504–509.
Weber T, Köster R (2013). Genetic tools for multicolor imaging in zebrafish larvae. Methods 62, 279–291.
Wegner W, Ilgen P, Gregor C, van Dort J, Mott AC, Steffens H, Willig KI (2017). In vivo mouse and live cell STED microscopy of neuronal actin plasticity using far-red emitting fluorescent proteins. Sci Rep 7, 11781.
Weinhard L, Bartolomei G, Bolasco G, Machado P, Schieber NL, Neniskyte U, Exiga M, Vadisiute A, Raggioli A, Schertel A, Schwab Y (2018). Microglia remodel synapses by presynaptic trogocytosis and spine head filopodia induction. Nat Comm 9, 1228.
Weissman T, Pan Y (2015). Brainbow: new resources and emerging biological applications for multicolor genetic labeling and analysis. Genetics 199, 293–306.
Westerfield M (2000). The Zebrafish Book: A Guide for the Laboratory Use of Zebrafish, Eugene: University of Oregon Press.
Worley MI, Setiawan L, Hariharan IK (2013). TIE-DYE: a combinatorial marking system to visualize and genetically manipulate clones during development in drosophila melanogaster. Development 140, 3275–3284.
Wu F, Van Rijn E, Van Schie BG, Keymer JE, Dekker C (2015). Multi-color imaging of the bacterial nucleoid and division proteins with blue, orange, and near-infrared fluorescent proteins. Front Microbiol 6, 607.
Xiong F, Obholzer ND, Noche RR, Megason SG (2015). Multibow: digital spectral barcodes for cell tracing. PLoS One 10, e0127822.
Yu D, Baird M, Allen J, Howe E, Matthew P (2015). A naturally-monomeric infrared fluorescent protein for protein labeling in vivo. Nat Methods 12, 763–765.
Yu D, Dong Z, Gustafson W, Ruiz-González R, Signor L, Marzocca F, Borel F, Klassen M, Makhijani K, Royant A, *et al*. (2016). Rational design of a monomeric and photostable far-red fluorescent protein for fluorescence imaging in vivo. Protein Sci 25, 308–315.
Zhong G, Wang H, Li Y, Tran MH, Farzan M (2017). Cpf1 proteins excise CRISPR RNAs from mRNA transcripts in mammalian cells. Nat Chem Biol 13, 839.